Response to editor's Comments:

Jiming Li et al. (Author)

We are very grateful for the editor's detailed comments, which helped us improve this paper significantly. Some grammatical errors already were corrected in the revision. Based on the editor's suggestions, we also added more explanations and scientific discussions in the section 4 to make the manuscript more clear. All changes already were marked by using yellow color in revised paper.

L31: drop "preliminary"

Response: We already removed it.

L36 and L38: replace standard deviation by another metric (mean absolute deviation positive/negative?) - since mean − 1 std dev is smaller than zero, impossible

Response: In revised paper, we added one sentence, "The result which the standard deviations are larger than mean values of cloud scale, was also found in the study of Zhang et al. (2014). They showed that the global mean Ac along-track horizontal scale is 40.2 km, but the standard deviation reaches 52.3 km. It is clear that the along-track horizontal scales of these cloud systems all have considerable variations globally" (See Line 368-373).

L40: specify with regard to what the 41% are considered

Response: In revised paper, we already added some descriptions in abstract and section 3.3 (see Line 38-42, Line 640-645).

L43: specify what the "entire multilayered cloud system" is

Response: We already replaced the "entire multilayered cloud system" with "all multilayered cloud systems" (see Line 44).

L49: this is probably 40 °N?

Response: We already corrected it, and it must be 40 °S (see Line 50).

L66: re-formulate "particularly significant" to more precisely say what is meant.

Response: We already re-formulated it in the revised paper (see Line 66-69).

L99: Also clarify the limits of ground-based radar.

Response: We already added the related descriptions of ground based radar in the introduction (see 106-109).

L103: "frequencies, respectively" since observers often dont see high, satellites not low clouds.

Response: We already revised it.

L104: why retrievals and radiative effects?

Response: Since passive satellite retrieval techniques are based on the typical single-layered cloud assumption, thus it is difficult to retrieve the exact cloud properties and cloud radiative effects of the multilayered cloud systems (see Line 104-106).

L105: should this read: single-layered?

Response: It must be "specific multilayered (or single-layered) cloud systems" (see Line 111).

L141: comma rather than slash between cirrus and cirrostratus

Response: We already corrected it (see 146).

L167: In my browser, the link does not work. Please correct.

Response: We already corrected it (see 172).

L266: More generally, it is the large-scale circulation that matters.

Response: we already revised it (see Line 271-275).

L287: "near 30°" a space is missing

Response: we already corrected it (see Line 287).

L295: "may even" please specify "over ocean"

Response: we already added this information (see Line 304).

L297: "under large-scale subsidence regions": where does this information stem from? it is not obvious from Table 1.

Response: we already deleted the somewhat vague expression in the revised paper (see Line 306).

L369: "cloud radiative effect": The spectral range needs to be specified (solar? terrestrial? net?)

Response: we already added the related information in the revised paper (See Line 202-207 and section 3.3).

L370: "during daytime": how is this averaged? Or is it instantaneous at overpass time? Specification needed.

Response: In this study, the cloud radiative effect only is the instantaneous net effects at the overpass time of the satellites during the daytime. We added the information in the section 2 (See Line 202-207).

L392: atmospheric heating of up to 3 Wm-2: from the numbers in L407 it seems 3 Wm-2 is rather the average effect, and Fig. 7 shows very large differences between toa and sfc. What is the actual range?

Response: In the revised paper, we added one figure as the supporting material (see Figure S1), and related descriptions are also added in the section 3.3 (see Line 403-411).
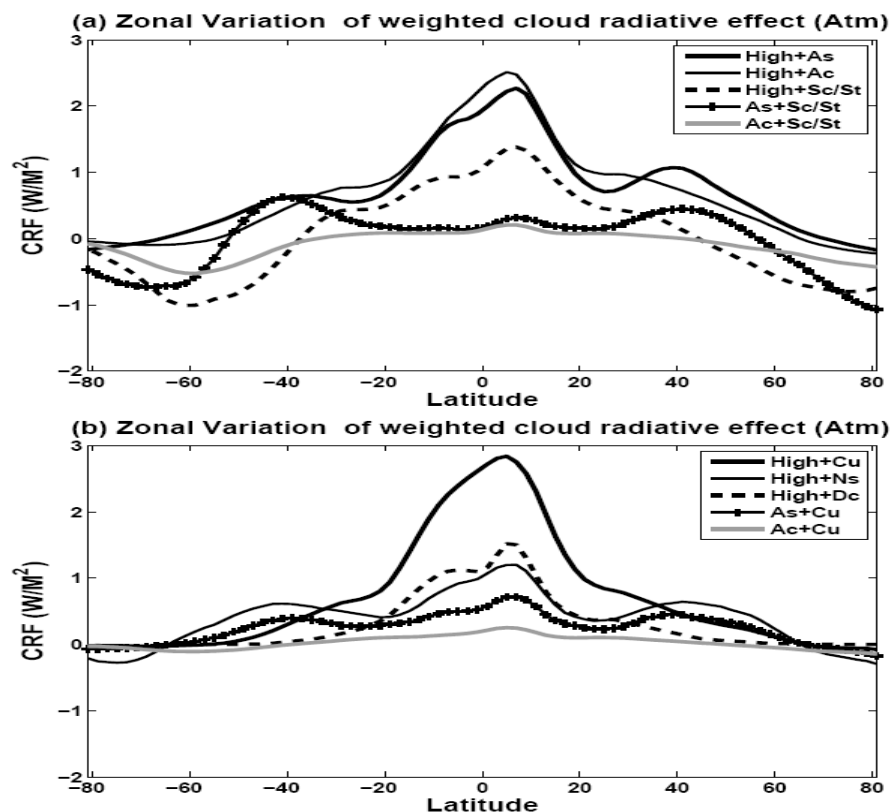

Fig. S1: Same with Figure5, but in the atmosphere during the daytime.

The Fig. S1 shows that the zonal variations of the instantaneous net cloud radiative effects of different multilayered cloud types in the atmosphere are very distinct. Most

of the multilayered cloud types heat atmosphere (their peak values range from 0.5 W/m^2 to 3 W/m^2) almost at all latitudes except As+Sc/St, Ac+Sc/St and High+Sc/St cloud systems, which cause a weak atmospheric cooling (peak value is approximately -1 W/m^2) at mid and high latitudes. In addition, statistical results also further show that the combined net CRE of the ten multilayered cloud types in the atmosphere decreases from the tropics to high latitudes, its value ranges ==from 13 W/m^2 (heating effect) to -3 W/m^2 (cooling effect).== The difference of radiative effect between TOA and surface in Figure 7 only is the combined effect of the ten multilayered cloud systems.

L396: "on a global scale": these are, however, in-cloud values, aren't they? Needs explanation.

Response: These values are the global mean instantaneous net radiative effects of the ten multilayered cloud systems (range from -100 W/m^2 to -350 W/m^2), they aren't the weighted radiative effects. (see 412-414).

L421: A brief discussion would be useful on the scale-dependency of the overlap parameter (linking back to chapter 3.3) and then a clarification at which scale this analysis is performed.

Response: we already added the related discussion and information in the section 4 (see Line 468-477, Line 485-488)), and the scale used in this study is 2 °×2 °.

L454: tend to be

Response: We already revised it.

L470: "rather than": this sentence is difficult to understand and needs reformulation

Response: we already re-formulated this sentence (see Line 503).

L475: considered better on which basis?

Response: We already revised it (see Line 495-497; 506-508).

L487: why "approximately"?

Response: We already corrected similar errors.

L590: A discussion would be useful on how the result, that minimum overlap tends to be a decent approximation in not few cases, might depend on observation limitations. Truely minimum overlap is what ISCCP or another passive sensor

would observe. Why do the active sensors also tend into this direction?

Response: We appreciate the insightful suggestion made by editor. In fact, negative overlap parameters indicate that fractions of cloud overlap are overestimated by random overlap assumption at mid and high latitudes of two hemispheres, and a tendency for an even more minimal degree of overlap than that predicted by the random overlap assumption is exist over there. Due to passive sensors (such as, ISCCP) usually fail to detect effectively the cloud overlap, thus minimum overlap is what ISCCP or another passive sensor would observe. However, why do the active sensors in our results and previous studies (Hogan and Illingworth, 2000; Mace et al., 2002) also tend into this direction over those regions? We consider the reason possible is as cloud features in one bigger grid box (here, $2°\times2°$) associated with vertical wind shears (or other dynamical factors in those regions) that are sloped in space to become more grouped together, thus trending toward increasing cloud cover over there. But, similar trend whether can be observed by active sensors in a smaller spatial scale (such as, $1°\times1°$) still needs to be confirmed in the future study by using this dataset.

L603: "more likely" than what?

Response: We already revised it (see Line 635).

L609: radiative contributions: the radiative effect numbers are in-cloud?

Response: We already revised it in the revised paper (see Line 641-645).

L1061 (Caption Fig. 5): please specify how the weighting is done, and whether it is in the solar or terrestrial spectrum, or net, and whether "during daytime" is averaged over a certain period (length of day?).

Response: Related information already was added in the caption Fig. 5.

L1120: specify "relative difference", probably "relative difference between real and random overlap"

Response: we already revised it.

1   A global survey of cloud overlap

2   based on CALIPSO and CloudSat measurements

3   Jiming Li,[1] Jianping Huang,[1,*] Knut Stamnes,[2]

4   Tianhe Wang,[1] Qiaoyi Lv[1], Hongchun Jin[1]

5   [1]Key Laboratory for Semi-Arid Climate Change of the Ministry of Education, College

6   of Atmospheric Sciences, Lanzhou University, Lanzhou, China

7   [2]Department of Physics and Engineering Physics, Stevens Institute of Technology,

8   Hoboken, NJ, USA

9

10   Running Head: Statistical properties of cloud overlap

11

12   *Corresponding author: Jianping Huang, Key Laboratory for Semi-Arid Climate

13   Change of the Ministry of Education, College of Atmospheric Sciences, Lanzhou

14   University, Lanzhou, Gansu 730000, China. (hjp@lzu.edu.cn)

15

16

17

18

19

20

21

22

23

24

25

Abstract

Using 2B-CLDCLASS-Lidar (Radar-Lidar) cloud classification and 2B-FLXHR-LIDAR radiation products from CloudSat over four years, this study evaluates the co-occurrence frequencies of different cloud types, analyzes their along-track horizontal scales and cloud radiative effects (CREs), and utilizes the vertical distributions of cloud types to evaluate cloud-overlap assumptions.

The statistical results show that high clouds, altostratus, altocumulus and cumulus tend to co-exist with other cloud types. However, stratus (or stratocumulus), nimbostratus and convective clouds are much more likely to exhibit individual features than other cloud types. On average, altostratus-over-stratus/stratocumulus cloud systems have a maximum horizontal scale (17.4 km), with a standard deviation of 23.5 km. altocumulus-over-cumulus has a minimum scale (2.8 km), with a standard deviation of 3.1 km. By considering the weight of each multilayered cloud type, we find that the global mean instantaneous net CREs of multilayered cloud systems during the daytime are approximately -41.3 W/m^2 and -50.2 W/m^2, which account for 40.1% and 42.3% of the global mean total net CREs at the top of the atmosphere (TOA) and at the surface, respectively. The radiative contributions of high-over-altocumulus and high-over-stratus/stratocumulus (or cumulus) in the all multilayered cloud systems are dominant due to their frequency.

Considering the overlap of cloud types, the cloud fraction based on the random overlap assumption is underestimated over vast oceans, except in the west-central Pacific Ocean warm pool. Obvious overestimations mainly occur over tropical and subtropical land masses. In view of an lower degree of overlap than that predicted by the random overlap assumption occur over the vast ocean, particularly poleward of 40 °S, the study therefore suggest that a linear combination of minimum and random overlap assumptions may further improve the predictions of actual cloud fractions for multilayered cloud types (e.g., As+St/Sc and Ac+St/Sc) over the Southern Ocean. The establishment of statistical relationship between multilayered cloud types and the environmental conditions (e.g., atmospheric vertical motion, convective stability and

wind shear) would be useful for parameterization design of cloud overlap in numerical models.

1. Introduction

As the most important regulators of the Earth's climate system, clouds significantly affect the radiation budget, the hydrological cycle and the large-scale circulation of the Earth (Hartmann et al., 1992; Stephens, 2005). However, because of incomplete knowledge of their underlying physical processes, clouds are still poorly represented in climate and weather models (Zhang et al., 2005) and are considered a major source of uncertainty in climate change predictions by GCMs (Cess et al., 1990).

Cloudiness is composed of a variety of types that are governed by different types of atmospheric motion and are associated with different microphysical properties; On the other hand, different cloud types have distinct cloud radiative effects and precipitation forms (Ackerman et al., 1988; Betts and Boers, 1990; Hartmann et al., 1992). However, multilayered cloud systems, in which two or more cloud types are simultaneously present over the same location but at different levels in the atmosphere, have been frequently reported by surface and aircraft observations (Tian and Curry, 1989). The frequent co-occurrences of different cloud types in the atmosphere increase the complexity of present cloud climatology studies. For example, the effects of individual cloud types on the surface and atmospheric radiation budgets depend on whether other clouds are also present above or below them. In addition, cloud overlap variations can significantly change atmospheric radiative heating/cooling rates, atmospheric temperatures, hydrological processes, and daily variability (Chen and Cotton, 1987; Morcrette and Jakob, 2000; Liang and Wu, 2005). Therefore, to improve radiation calculations of climate prediction models, understand cloud physical processes, and evaluate the schemes for generating clouds in those models, it is necessary to know the amount and distribution of each cloud type, particularly a detailed description of the co-occurrence of different cloud types and their statistical

84   properties.

85   Until recently, many related studies on cloud types and cloud overlap, which are

86   based on several fundamentally different types of passive observational datasets

87   (typically the International Satellite Cloud Climatology Project (ISCCP) and surface

88   observer reports), have focused on the geographical distributions and long-term

89   variations of cloud types (e.g., Rossow and Schiffer, 1991; Rossow and Schiffer,1999;

90   Hahn et al., 2001; Warren et al., 2007; Eastman et al., 2011; Eastman et al., 2013),

91   cloud radiative effects (Hartmann et al., 1992; Chen et al., 2000; Yu et al., 2004),

92   cloud-property retrievals in multilayered clouds using multi-channel measurements

93   from passive sensors (Chang and Li, 2005a, Chang and Li, 2005b; Huang et al., 2005;

94   Huang et al., 2006a; Huang et al., 2006b; Minnis et al., 2007), and the statistics of

95   cloud overlap based on surface weather reports and measurements from ground-based

96   cloud radar (Warren et al., 1985; Hogan and Illingworth, 2000; Minnis et al., 2005).

97   However, these studies have different limitations and uncertainties. First, passive

98   detection methods and cloud-classification algorithms generally fail to detect

99   multilayered clouds effectively. Such as, the existence of overlapping cloud layers

100   may obscure the upper-level clouds from the perspective of a ground-based weather

101   reporter, and lower clouds may be hidden from the view of a passive satellite. As a

102   result, surface observer reports and ISCCP significantly underestimate high and low

103   cloud frequencies, respectively, and introduce significant biases into the trend analysis

104   of cloud cover, retrievals of cloud properties and evaluations of cloud radiative effects

105   for the multilayered cloud systems since passive satellite retrieval techniques are

106   based on the typical single-layered cloud assumption. Second, although the cloud

107   properties can be retrieved relatively accurately from ground based lidar or radar

108   signals, only one-dimensional observations are possible, and the sites are sparsely

109   distributed, almost non-existent over the oceans. Third, most of these studies are

110   limited to specific locations and time periods or specific multilayered (or

111   single-layered) cloud systems. Systematic studies on the statistical co-occurrence of

112   different cloud types on a global scale still have received far less attention.

113   Fortunately, the millimeter-wavelength cloud-profiling radar (CPR) on CloudSat

(Stephens et al., 2002) and the cloud-aerosol lidar with orthogonal polarization (CALIOP) (Winker et al., 2007) on CALIPSO (launched in late April 2006) provide an unprecedented opportunity for detailed studies on the three-dimensional structures of clouds on a global scale. Since mid-June 2006, CALIPSO and CloudSat data have been widely used to investigate the three-dimensional distributions and structures of hydrometeors and to improve the cloud-overlap assumption used in GCMs (e.g., Barker, 2008; Luo et al., 2009; Kato et al., 2010; Li et al., 2011). By using a radar-only cloud-classification product (i.e., the 2B-CLDCLASS dataset from CloudSat), Sassen and Wang (2008) presented the geographical distributions and global average frequency of each cloud type. In this study, we investigate the co-occurrence frequencies of different cloud types and analyze their along-track horizontal scales and radiative effects using the latest cloud-classification and radiative-flux products based on the combined measurements of the two active sensors mentioned previously. Finally, we perform a preliminary evaluation of how well cloud-overlap assumptions characterize the overlap of two apparently separate cloud types. Although some statistical results reasonably agree with previous studies, new insights are achieved in this investigation. These new results will hopefully be useful for future GCMs evaluations and improvements.

The study is organized as follows. The dataset for the research is described in Section 2. Section 3 provides the zonal distributions and global statistics of the co-occurrence frequencies of cloud types and discusses their along-track horizontal scales and radiative effects. An evaluation of the performance of cloud-overlap assumptions based on the co-occurrence frequencies of cloud types is presented in Section 4.

2. Data

In the following study, four years (2007-2010) of data from the latest release of the CloudSat 2B-CLDCLASS-Lidar (version 1.0) product (i.e., Radar-Lidar cloud classification) and the 2B-FLXHR-LIDAR product are collected to analyze cloud types and discuss their co-occurrence frequencies, horizontal scales and radiative effects.

144   The ISCCP uses a combination of cloud-top pressure and cloud optical depth to

145   classify clouds into cumulus, stratocumulus, stratus, altocumulus, altostratus,

146   nimbostratus, cirrus, cirrostratus, and deep convective clouds. However, traditional

147   surface observations identify clouds by using basic features (e.g., base height,

148   horizontal and vertical dimensions, and precipitation types) of the major cloud types

149   (World Meteorological Organization, 1956; Parker, 1988; Moran et al., 1997). Based

150   on these basic cloud characteristics, Wang and Sassen (2001) classified cloud types

151   into eight classes by combining the range capabilities of active sensors (radar and

152   lidar) and the auxiliary measurements from the other passive sensors (e.g., infrared

153   and microwave radiometers); they further indicated the overall agreement

154   (approximately 70%) between the results from their algorithm and the surface visual

155   observations from the Southern Great Plains (SGP) CART site.

156   Based on the algorithm presented by Wang and Sassen (2001), the Radar-Lidar

157   cloud classification identifies the cloud types using two steps. First, combined radar

158   and lidar cloud-mask results are used to find a cloud cluster according to cloud

159   persistence in the horizontal and vertical directions. By performing the cloud

160   clustering analysis, a CloudSat granule may be divided into a number of cloud

161   clusters, depending on the cloud systems present. Once a cloud cluster is found, the

162   cloud height and phase, maximum effective radar reflectivity factor (Ze) and

163   temperature, and the occurrence of precipitation are determined. Second, the cluster

164   mean properties and spatial inhomogeneities, in terms of the cloud-top heights and

165   maximum signals of the radar and lidar, are sent to a fuzzy classifier to classify the

166   cluster into one cloud type with an assigned confidence level. To improve the

167   classification flexibility, a combination of rule-based and fuzzy-logic-based

168   classification is used in this algorithm. The cloud-phase determination is based on

169   rules, and the cloud-type classification is mainly based on fuzzy logic (see Wang et al.,

170   Level 2 Combined Radar and Lidar Cloud Scenario Classification Product Process

171   Description and Interface Control Document, version 1.0, 2013, available at

172   http://www.cloudsat.cira.colostate.edu/dataSpecs.php?prodid=12&pvid=12).   The

173   cloud types provided by this product (version 1.0) include high clouds (High),

altostratus (As), altocumulus (Ac), stratus (St), stratocumulus (Sc), cumulus (Cu), nimbostratus (Ns) and deep convective (Dc) clouds. The High cloud type includes cirrus, cirrocumulus and cirrostratus, and the Cu cloud type represents cumulus congestus and fair weather cumulus. Following the study of Sassen and Wang (2008), we also combine two cloud types (St and Sc) into St+Sc in the present study. By combining the unique complementary capabilities of the cloud profile radar (CPR) of CloudSat and the space-based polarization lidar (CALIOP), some CPR weaknesses (e.g., high surface contamination in the lowest three to four vertical bins of the CPR and a lower sensitivity to optically thin clouds) are minimized in the latest Radar-Lidar cloud classification product; thus, the identification of High (cirrus or cirrostratus) and low cloud types (such as St, Sc and Cu) is significantly improved in the 2B-CLDCLASS-Lidar product.

By using CloudSat microphysical retrievals, a combined CloudSat/CALIPSO cloud mask and lidar-based aerosol retrievals as inputs for a broadband, two-stream, plane-parallel, adding-and-doubling radiative transfer model, the 2B-FLXHR-LIDAR product provides calculated radiative fluxes and atmospheric heating rates at 240 m vertical increments (Henderson et al., 2013). Incorporating the radiative influence of optically thin and low clouds that were undetected by CloudSat significantly improved the agreement between the 2B-FLXHR-LIDAR calculations and observations from the Clouds and the Earth's Radiant Energy System (CERES) experiment. Henderson et al. (2013) showed that the global mean outgoing shortwave radiation (OSR) and outgoing longwave radiation (OLR) estimated from the collocated CERES observations and 2B-FLXHR-LIDAR calculations agree within 4 and 5 W/m^2, respectively, with root-mean-square differences of 6 W/m^2 and 16 W/m^2 on monthly/5 ° scales. Because the passive sensors largely fail to resolve the cloud overlap in the vertical, the 2B-FLXHR-LIDAR product derived from these two active sensors is considered a vital dataset for examining the radiative heating features in the atmosphere and for studying the variations in fluxes and heating rate caused by vertically overlapping clouds (L'Ecuyer et al., 2008; Haynes et al., 2013). In this investigation, we only provide the results of the net radiative effect of different

multilayered cloud types at the TOA and at the surface during the daytime by using the 2B-FLXHR-LIDAR. However, it needs to further explain that the radiative effects of different cloud types only are the instantaneous effects at the overpass time of the satellites during the daytime in this study.

The following cloud parameters in the 2B-CLDCLASS-Lidar product are used in this study: cloud layer (CL) and cloud layer type (CLTY). In the 2B-FLXHR-LIDAR product, only the TOACRE (cloud radiative effect at the TOA) and BOACRE (cloud radiative effect at the surface) are used. Here, we consider one data profile as a multilayered (or single-layered) cloud profile when two or more cloud layers (or only one layer) are present within the vertical profile based on the parameter "cloud layer". To map the regional variability in the studied variable, we group the global area into $2°\times2°$ grid boxes to collect a sufficient number of samples in each grid box. Following the definitions of cloud fraction and cloud amount proposed by Hagihara et al. (2010), the cloud-type fractions and amounts in a given grid box are defined as the number of particular cloud-type profiles divided by the number of total sample profiles and the total cloud profiles within this box, respectively. For example, the cloud fraction for multilayered clouds is the ratio of the number of multilayered cloud profiles to the number of total sample profiles in a given grid box. In this investigation, we only provide the annual average cloud properties of different overlapping cloud types with small seasonal variations. In addition, comparisons of the four-year average cloud fractions for different cloud types between daytime and night-time are provided in tables. Notably, the day-night comparisons of cloud fractions are only represented by the two overpass times of the satellites. The full diurnal cycle cannot be captured by CALIPSO and CloudSat. Sassen et al. (2009) showed that the observed day-night variations in cirrus observed by CALIPSO mostly reflect real cloud processes, even when the strong solar noise signature impacts the comparisons of cloud types between day and night, particularly for cirrus. For other cloud types, the uncertainty caused by the daylight noise for lidar may be smaller. Thus, the calculated annual mean cloud fractions for different cloud types in this investigation are reliable.

3. Simultaneous co-occurrence of different cloud types

3.1. Zonal distributions of overlapping clouds

Multilayered cloud systems frequently occur in the atmosphere. Our statistical results show that the seasonal variations in multilayered cloud percentages are small, and the seasonal globally averaged values range between 25% and 28%. These results are comparable to the multilayered cloud fractions (approximately 27%) from the Geoscience Laser Altimeter System (GLAS) (Wylie et al., 2007). Furthermore, we plot the global and zonal distributions of the annually averaged multilayered cloud fractions (see Fig.1). In Fig.1a, the high-value and low-value centers of the multilayered cloud fractions are very obvious. For example, equatorial central South America, western Africa, Indonesia and the west-central Pacific Ocean warm pool are typical high-value centers. There are three obvious peaks in the zonal mean patterns (Fig.1b): one major peak occurs in the tropics, and two minor peaks occur in the midlatitudes; two local minima occur in the subtropics. The local maximum during spring (thick, black line) in the northern midlatitudes may be the result of misidentifying high-level dust transport as high ice clouds or the result of the actual influences of dust on ice nucleation (Chen et al., 2010; Yu et al., 2012; Yuan and Oreopoulos, 2013).

In all multilayered clouds, we further identify the most frequently multilayered cloud systems (annually) and provide their zonal distributions (Fig. 2). Note that the overlap of the same cloud type (e.g., High+High) is not important in numerical climate simulations because these clouds have similar cloud properties and temperatures. Thus, treating these clouds as a single layer may not introduce serious errors into the calculation of the cloud properties (Wang and Dessler, 2006). In addition, the overlap of specific two cloud types in any three or more layer cloud systems (e.g., High+As+Cu) is also included in statistical results of their occurrence frequencies. But, only two layer cloud systems is used when we calculate the weighted cloud radiative effect of specific two cloud types-overlap in section 3.3. Fig. 2 clearly indicates that the zonal patterns of different combinations of cloud types are very different. For example, multilayered cloud systems that include high clouds

either have one peak in the tropics (High+Ac and High+Cu) or three peaks in the tropics and midlatitudes (High+St/Sc, High+Ns and High+As). The high clouds that represent the major peak in the tropics may be caused by large-scale ascent or by dissipating deep convection. However, gentle large-scale ascent and ice cloud production within frontal convection are likely responsible for the two minor peaks of the multilayered cloud systems along midlatitude storm tracks. In addition to these combinations of cloud types, As-over-stratiform clouds or Ac-over-stratiform clouds also tend to be concentrated in the midlatitudes (60° and poleward). In fact, the distributions of clouds in different geographical regimes depend on the large scale circulation, but the environmental factors in same regimes, such as sea surface temperature, lower tropospheric stability, and vertical velocity are also important to the occurrences of different cloud types (Klein and Hartmann, 1993; Norris and Leovy, 1994). By studying the relations between various cloud types and the sea surface temperature of the tropical oceans, Behrangi et al. (2012) indicated that as the SST increases, the fraction of multilayered clouds increases up to a SST of 303 K and then decreases for SSTs greater than 303 K. The ranges of SSTs are very different for different combinations of cloud types, e.g., high clouds over St/Sc or Ns clouds tend to occur between 292 and 294 K, but high clouds over Ac, As or Cu clouds tend to occur between 302 and 304 K, even though almost all of the clouds have major peak values in the tropics. In addition, Yuan and Oreopoulos (2013) indicated that the vertical velocity of large-scale pressure systems has a negative correlation with the percentage of multilayered cloud systems. Strong subsidence favors low cloud formation and suppresses ice cloud generation; thus, multilayered clouds are infrequent over major Sc-dominated oceanic areas at latitudes near 30°.

However, multilayered cloud systems are very difficult to detect by passive satellites (such as ISCCP) and by surface weather reporters, particularly during the night-time and for cloud systems that include very thin cirrus (Sassen and Cho, 1992; Liao et al., 1995). For example, when a high-level transparent cirrus cloud overlies a boundary layer stratus cloud, the retrieved cloud-top heights typically lie between the cirrus and stratus cloud heights (e.g., Baum and Wielicki, 1994), leading to the

misinterpretation of cloud types by ISCCP. For cloud property retrievals, the influence of liquid water clouds and precipitation on the radiances observed at the TOA is also one of the greatest impediments to determining the cloud ice mass for multi-layered systems that include ice clouds above water clouds (Huang et al., 2006a).

3.2. Global statistics of cloud overlap

The global average percentage overlap of different combinations of cloud types over land or ocean during the daytime and night-time are provided in Tables 1 and 2, respectively. These tables show that high clouds, As, Ac and Cu tend to co-exist with other cloud types, regardless of the time of day or surface type. The frequency of High-over-Ac over ocean may even exceed the frequency of single-layered Ac clouds over ocean, indicating that these two types actually exhibit a stronger meteorological association. However, St/Sc and Ns are much more likely to exhibit individual features than other types, particularly St/Sc over the ocean. Convective clouds are also typically in single layers. Although Cu form in unstable air and As form in stable air, a small percentage of overlap occurs. Globally, 44% (50%) and 35% (39%) of low clouds (St/Sc +Cu) over land and ocean during the daytime (night-time) are overlapped by other cloud types aloft. Approximately 23% (26%) and 20% (25%) of low clouds over land and ocean during the daytime (night-time) are connected with high clouds. These percentages are comparable to those (approximately 30%) presented by Yuan and Oreopoulos (2013). Notably, high clouds also include cirrostratus and cirrocumulus; thus, the percentage of overlap of deep convection below high clouds is approximately 29%, which is larger than the percentage (approximately 24%) of cirrus-over-convection clouds based on ICESat/GLAS (Geoscience Laser Altimeter System) (Wang and Dessler, 2006).

Based on the above figures and tables, we plot the global distributions of the annual mean dominant cloud types and their cloud fractions. Here, the cloud types include all single-layered and multilayered cloud systems (see Fig. 3a-3b). Fig. 3c-3d shows that the global distributions of the annual mean cloud types (only for multiple dominant clouds) and corresponding cloud amounts. Based on Fig.3a-3b, St/Sc is the

324   dominant cloud type worldwide, particularly over the ocean. High clouds are mainly

325   concentrated in the tropics and subtropics. In addition, over Antarctica, the most

326   frequent cloud type is As. These results are in reasonable agreement with the findings

327   based on the ISCCP D1 dataset (Doutriaux-Boucher and Seze, 1998). However, Fig.

328   3a-3b also shows that As prevails over the arid/semi-arid land in the Northern

329   Hemisphere, such as northwestern China and North America. In contrast, Ac is

330   dominant over the arid/semi-arid land of the Southern Hemisphere, such as Australia

331   and southern Africa. However, not all of these features are observed by

332   Doutriaux-Boucher and Seze (1998) using the ISCCP D1 dataset. In fact, the obvious

333   regional and seasonal variations in Ac and As are possibly related to the frequency of

334   dust activities (Choi et al., 2009). In addition, over some deserts (such as the Sahara

335   Desert), the most prevalent cloud type is low-level clouds (St/Sc) according to the

336   ISCCP D1, as opposed to the high clouds in our results. This discrepancy may be due

337   to inadequate identification of airborne dust, such as the ISCCP misclassifying dust as

338   low-level clouds, as suggested by the low values of the effective droplet radius

339   reported by Han et al. (1994) over these regions.

340   Generally, the High-over-St/Sc and High-over-Cu cloud systems are more

341   common over the vast oceans of the tropics and midlatitudes, while High-over-Ac

342   cloud systems tend to exist over land at the same latitudes (see Fig. 3c). Notably,

343   As-over-Cu only occurs over northwestern China. In addition, the As-over-St/Sc

344   cloud systems are dominant in the high latitudes. Fig. 3d shows the multilayered

345   cloud-type amount, defined as the ratio of the cloud fraction of one multilayered cloud

346   combination to the cloud fraction of total multilayered cloud systems. In addition, we

347   note that some multilayered cloud systems (High-over-St/Sc) exist over the major

348   Sc-dominated oceanic areas, which are generally unfavorable for upper-level cloud

349   formation due to persistent strong subsidence. The major source of high clouds is

350   topography-driven gravity wave activity, advection from neighboring tropical

351   convection centers, such as the Amazon Basin or the Congo Basin, or ascent

352   associated with midlatitude fronts.

353   **3.3. Along-track horizontal scales and radiative effects of cloud overlap**

The horizontal scale of a multilayered cloud system along the CALIPSO/CloudSat track is determined by calculating the number of continuous profiles (N), in which each profile includes a vertical column with a particular combination of cloud types. Considering the 1.1 km along-track resolution of CPR measurements, the along-track scale (L in km) of a multilayered cloud system is $L = N \times 1.1$ (Zhang et al., 2014).

Fig. 4a-4d presents the zonal variation in the along-track horizontal scales of clouds in the multilayered cloud systems and their probability distribution functions (PDFs). As shown in Fig. 4a-4b, the High+St/Sc, As+St/Sc, High+Ns and High+Dc cloud systems have obvious zonal variations. High+St/Sc and As+St/Sc have minimum scales (approximately 10 km) in the tropics and maximum scales (up to 20 km) poleward of $40°$ (i.e., along the storm tracks). However, the along-track horizontal scales of High+Ns and High+Dc decrease from the tropics to the poles. The zonal variations in the scales of other clouds systems are small, particularly for High+Cu, As+Cu and Ac+Cu (approximately 3 km). We also provide the global average along-track horizontal scales and standard deviation (STD) of these cloud systems in Fig. 4c-4d. Generally, As+St/Sc has a maximum scale (17.4 km) and STD (23.5 km), while Ac+Cu has a minimum scale (2.8 km) and STD (3.1 km). The result which the standard deviations are larger than mean values of cloud scale, was also found in the study of Zhang et al. (2014). They showed that the global mean Ac along-track horizontal scale is 40.2 km, but the standard deviation reaches 52.3 km. It is clear that the along-track horizontal scales of these cloud systems all have considerable variations globally. By assuming a typical grid resolution of $1°$ in global climate models, we find that all multilayered cloud types cannot be resolved by global climate models. The multilayered cloud systems that include Cu (such as High+Cu, Ac+Cu and As+Cu) are not even captured by regional climate models with higher grid resolutions (approximately 15 km).

Furthermore, Fig. 5a-5b shows the zonal distributions of the instantaneous net TOA cloud radiative effects (CREs) of these multilayered cloud systems at overpass time of satellite during the daytime. In addition, we also provide the zonal distributions of weighted instantaneous net CREs by considering the frequency of

occurrence of each cloud type during the daytime only (Fig. 5c-5d). Although the zonal distributions of the net CREs for these cloud systems are similar, i.e., decrease from the tropics to high latitudes, the radiative effects can be grouped into several distinct classes. For example, middle-over-low (such as As+Sc/St and As+Cu) cloud systems have comparable radiative effects (maximum value of -300 W/m^2), while high-over-low (such as High+Sc/St and High+Cu) cloud systems have small radiative effects (maximum value of -150 W/m^2). By considering the weight of each multilayered cloud type, we find that their contributions to the cloud radiative effect of the whole multilayered cloud system are different (Fig. 5c-5d). In the tropics, High+Ac and High+Cu contribute -9 W/m^2 and -8 W/m^2, respectively, to the net radiative effects. Other cloud types have obvious zonal distributions, and their contributions range from 0 to -6 W/m^2. In mid-high latitudes, some mid-over-low (such as As+Sc/St) cloud systems are more important to the regional energy balance, particularly over the Southern Ocean regions. Similar to Fig. 5, Fig. 6 presents the surface-based results during the daytime. In summary, the trends are similar, but all cloud types have larger radiative effects at the surface than at the TOA; specifically, the effect is an obvious surface cooling. Clearly, the energy differences in the net cloud radiative effects between the surface and the TOA are persistent and may significantly change the atmospheric radiative heating/cooling rates and temperature. However, the zonal variations of the instantaneous net CREs in the atmosphere show that the radiative impacts are very distinct for the different multilayered cloud types (see Figure S1). Most of the multilayered cloud types heat atmosphere (their peak values range from 0.5 W/m^2 to 3 W/m^2) almost at all latitudes except As+Sc/St, Ac+Sc/St and High+Sc/St cloud systems, which cause a weak atmospheric cooling (peak value is approximately -1 W/m^2) at mid and high latitudes. In addition, statistical results also further show that the combined net CRE of the ten multilayered cloud types in the atmosphere decreases from the tropics to high latitudes, its value ranges from 13 W/m^2 (heating effect) to -3 W/m^2 (cooling effect).

Fig. 7a-7b shows the global mean instantaneous net radiative effects of the ten multilayered cloud systems range from -100 W/m^2 to -350 W/m^2, except for High+Dc

414   (the black dots are the mean values and the lines represent the standard deviation). In

415   Fig. 7c-7d, the black bars represent the weighted global mean instantaneous net

416   radiative effects of each cloud type at the TOA and surface. By combining the all

417   single-layered and multilayered cloud systems, the global mean total net CREs are

418   approximately -103.1 W/m^2 and -118.8 W/m^2 at the TOA and at the surface,

419   respectively. The all multilayered cloud systems contribute approximately 40.1%

420   (-41.3 W/m^2) and 42.3% (-50.2 W/m^2) to the global mean total net CREs at the TOA

421   and at the surface, respectively. Clearly, the existence of a multilayered cloud system

422   is important to Earth's radiative energy balance. A further analysis shows that all

423   two-layered and three-layered (or more layers) cloud systems contribute

424   approximately -27.2 W/m^2 (-33.1 W/m^2) and -14.1 W/m^2 (-17.1 W/m^2), respectively,

425   to the total cloud radiative effects at the TOA (surface). However, the radiative effects

426   of ten multilayered cloud types in our study are -22.7 W/m^2 and -27.1 W/m^2 at the

427   TOA and at the surface (a contribution of 22%). High+Ac and High+Sc/St (or Cu)

428   have relatively smaller effects than High+Dc and Ac+Sc/St (or Cu), but their

429   contributions to the cloud radiative effect of the all multilayered cloud systems are

430   highest because of their more frequent occurrence, larger weights (see the gray line in

431   Fig. 7c-7d), and distribution from the tropics to the midlatitudes (Fig. 3). However,

432   the other cloud types may be important to regional cloud radiative effects. For

433   example, mid-to-upper level clouds frequently coexist with boundary layer clouds

434   (e.g., As+St/Sc and High+St/Sc) over the Southern Ocean; thus, mid-atmosphere

435   cloudiness is overestimated by ISCCP and is partially responsible for the TOA

436   shortwave radiation bias in the climate models over this region (Haynes et al., 2011).

437 **4. Evaluation of cloud-overlap assumptions based on cloud types**

438   Based on the advantages of the two active sensors, we preliminarily evaluate

439   how well the cloud-overlap assumptions can characterize the overlap of two

440   apparently separate cloud types using the 2B-CLDCLASS-Lidar cloud type product.

441   The cloud overlap assumption has been widely used to describe the actual vertical

442   distribution of clouds and the parameterization of the total cloud fraction in a given

443   model grid box. Several basic cloud-overlap assumptions have been proposed, such as

444   maximum, random, random-maximum and minimum overlaps (Hogan and

445   Illingworth, 2000). The most common cloud-overlap scheme in current GCMs is

446   called "random-maximum" overlap, which assumes that cloud layers separated by

447   clear layers are randomly overlapped, while vertically continuous cloud layers have

448   maximum overlap (Stephens et al., 2004). When the cloud fractions of the upper and

449   lower layers are C_1 and C_2, the total cloud fractions of the two cloud layers based on

450   the overlap assumptions are given by:

451   $$C_{random}=C_1+C_2-C_1\times C_2,$$

452   $$C_{max}=\max(C_1, C_2), \text{ and}$$

453   $$C_{min}=\min(1, C_1+C_2). \tag{1}$$

454   In addition, if we know the actual overlap fraction $C_{overlap}$, then the observed total

455   cloud fraction C_{real} can be written as:

456   $$C_{real}=C_1+C_2-C_{overlap} \tag{2}$$

457   However, Hogan and Illingworth (2000) proposed a simpler and more useful

458   expression for the degree of cloud-layer overlap (exponential random overlap). In the

459   expression, the mean observed cloud fraction of two cloud layers can be determined

460   by the linear combination of the maximum and random overlap in terms of an

461   "overlap parameter" a,

462   $$C_{real}=a\times C_{max}+(1-a)\times C_{random} \tag{3}$$

463   Here, the overlap parameter a is considered a function of the layer separation, and

464   related to the vertical resolution and the horizontal domain size. $a=0$ is random

465   overlap and $a=1$ is the maximum overlap. As C_{real} increasingly departs from C_{max}

466   (trending toward C_{min}), a becomes negative, indicating a tendency for an even lower

467   degree of overlap than that predicted by the random overlap assumption. In fact,

468   previous studies already have shown that cloud overlap parameter is sensitivity to

469   spatial scale of GCMs grid box. For example, Hogan and Illingworth (2000) found

470   that a tends to increase with decreasing spatial and temporal resolution (that is, with

471   an increasing vertical and horizontal scale of GCMs), but one interesting finding is

472   that, with a temporal resolution of 3 hour (that is, horizontal scale of 216 km in their

473   study) and a level separation of between 6 and 8 km, a falls to -0.1. Mace et al. (2002)

474 also found an increase in a with decreasing temporal resolution at all sites but the

475 southern Great Plain (SGP) site while they find a decrease in a with decreasing spatial

476 resolution. However, Naud et al. (2008) found a decrease in a with increasing spatial

477 resolution by analyzing the cloud overlap at SGP site for the winter months. These

478 studies further implied that the degree of cloud overlap also may depend on the other

479 factors, such as, atmospheric vertical motion, convective stability and wind shear in

480 different seasons besides vertical resolution and the horizontal domain size (Mace et

481 al., 2002; Naud et al., 2008). For example, vertically continuous clouds tend to be

482 more maximally overlapped in the presence of vertical motion in midlatitudes and

483 decreased convective stability in the Tropics. However, large wind shears were found

484 to increase the randomness of the overlap, with overlap becoming less than random in

485 some cases ($a<0$). What changes from one high to low horizontal resolution is

486 actually the increase of number of samples, which in turn may affect the averaged

487 values of the vertical velocity, convective stability and wind shear, thus further effect

488 the way cloudy layers overlap.

489 Based on several months of data from ICESat/GLAS observations, Wang and

490 Dessler (2006) showed that overlap differences between the observed and random

491 overlaps exist when describing the actual overlap of two separated cloud types

492 (vertical separation >0.5 km). However, the authors' work focused on the tropics and

493 was limited to simple cloud classifications using space-based lidar. We expand the

494 study by Wang and Dessler (2006) by employing a global-scale analysis and a more

495 complete cloud classification; the overlap of two separate cloud types (here, vertical

496 separation >0.24 km at least) in each combination of cloud types in each grid box is

497 determined. Moreover, we evaluate the performances of the random overlap

498 assumption and calculate the overlap parameter a for each multilayered cloud type in

499 each $2°\times2°$ grid box.

500 We first group each multilayered cloud system. For example, for the all High+Cu

501 multilayered cloud systems in the same $2°\times2°$ grid box, we consider two layers and

502 group all high clouds into the upper layer and all cumulus clouds into the lower layer,

503 regardless of the vertical separation between these two types and their heights. Then,

504 four possible values for the combined total cloud fraction of the two cloud types at

505 different layers are calculated by assuming random overlap, maximum overlap,

506 minimum overlap and actually observed overlap. Because random cloud overlap is

507 considered a better characterization of cloud overlap behavior than minimum overlap

508 and maximum overlap when two cloud layers separated by clear layers, we only

509 provide the difference in the cloud fractions between random overlap and actually

510 observed overlap. Finally, the overlap parameter a for each multilayer in each grid is

511 calculated based on Eq. (3). Notably, because we do not group multilayered cloud

512 types into multiple layers according to the vertical separation of two types, only one

513 value for the overlap parameter a for each multilayered cloud system in each grid is

514 obtained. a may be considered the mean value of all overlap parameters at different

515 layer separations. Here, we define the relative difference (RD) between the random

516 and actual overlap for one of the multilayered cloud types as:

517 $$RD=(C_{random}-C_{real})/C_{real} \tag{4}$$

518 In addition, the cumulative relative difference (CRD) between the random and actual

519 overlap for all multilayered cloud types (here, 17 different combinations of different

520 cloud types are considered) in each 2°×2° grid box is given by:

521 $$CRD = \sum_{i=1}^{17} RD^i \times w^i \qquad i=1, 2, 3 \ldots, 17 \tag{5}$$

522 Similar to the definition of CRD, we define the cumulative overlap parameter (COP)

523 in each 2°×2° grid box as:

524 $$COP = \sum_{i=1}^{17} a^i \times w^i \qquad i=1, 2, 3 \ldots, 17 \tag{6}$$

525 where w is the weight coefficient for one multilayered cloud type in each 2°×2° grid

526 box as follows:

527 $$w^i = f^i / \sum_{i=1}^{17} f^i \qquad i=1, 2, 3 \ldots, 17 \tag{7}$$

528 f is the cloud fraction of each multilayered cloud type in every grid box.

529 Fig. 8a-8b shows the zonal distributions of the relative differences between the

530 random and actual overlap for ten of the main multilayered cloud types and the

531 cumulative relative differences for all multilayered cloud types (gray line). The results

532 show that differences exist, even though the random-cloud-overlap assumption is

533 thought to better describe cloud-overlap behavior than other schemes when the cloud

534 layers appear to be separate. The cloud fractions based on the random-overlap

535 assumption are underestimated for High+St/Sc, As+St/Sc and Ac+St/Sc at all

536 latitudes; these differences can exceed -5%. The cloud fraction of the High-over-Ac

537 system is overestimated at all latitudes. The peak values of the difference are mainly

538 located in mid- and high- latitudes in both hemispheres and are up to 5%. For other

539 types, the relative differences are smaller and change with latitude. In summary, the

540 cumulative relative difference of all multilayered cloud types is small (gray lines), and

541 almost values are negative at all latitudes. In Fig. 8c-8d, we further show the zonal

542 distributions of the overlap parameter for ten of the main multilayered cloud types and

543 the cumulative overlap parameter of all multilayered cloud types. Clearly, the overlap

544 parameters for High+St/Sc, As+St/Sc and Ac+St/Sc at all latitudes are negative,

545 indicating a C_{real} departure from C_{max} (trending toward C_{min}) and a tendency for an

546 even lower degree of overlap than predicted by the random overlap assumption. Thus,

547 the linear combination of maximum and random overlap assumptions is problematic

548 due to the negative overlap parameters in those regions, where the three multilayered

549 cloud types mentioned above are dominant, particularly over the major Sc-dominated

550 oceanic areas. However, the overlap parameters are positive for High+Ns and

551 High+Ac. Thus, C_{real} has a value between C_{max} and C_{random}, and the exponential

552 random overlap can predict the actual overlap of these two types very well. These

553 results are intuitive, as cloud types are governed by different types of atmospheric

554 motion and state. The formation of cumuli-form clouds may be related to the strong

555 ascent or convectively unstable which result in clouds that increase in height more

556 quickly, and increasing the degree of overlap with other cloud types. However,

557 random or minimum overlap occurs preferentially in regions of subsidence or

558 convective stability (favors strati-form cloud). Therefore, it is not difficult to

559 understand why the zonal distributions of cloud overlap parameters are very different

560 for similar cloud overlap systems (e.g., middle-over-low). For example, the overlap

561 parameters of As+St/Sc and Ac+St/Sc over the Southern Ocean are obviously distinct

562 from As+Cu and Ac+Cu. In summary, the cumulative overlap parameters of all

563   multilayered cloud types (gray lines) are negative at nearly all latitudes. However, two

564   points still require further interpretation. First, the cumulative overlap parameters in

565   the tropics and in the Northern Hemisphere have small values (and possibly positive

566   values); thus, random overlap or exponential random overlap is representative of the

567   actual conditions. Second, in the Southern Hemisphere, the cumulative overlap

568   parameters trend toward C_{min}; thus, a better prediction using random overlap or

569   exponential random overlap is difficult. This finding partially explains why the

570   climate model errors in the TOA fluxes over the Southern Ocean are the largest

571   (Trenberth and Fasullo, 2010). Based on the global results from this study, we also

572   further support the findings of Naud et al. (2008) that factors such as dynamics could

573   be connected to the way cloudy layers overlap. As a result, we suggest that a linear

574   combination of minimum and random overlap assumptions may further improve the

575   predictions of real cloud fractions for the multilayered cloud types in the Southern

576   Hemisphere (e.g., As+St/Sc and Ac+St/Sc), particularly poleward of 40°S over the

577   ocean. However, only three cloud types (e.g., low-level marine stratus, convective

578   cloud and layered cloud) are diagnosed by the cloud scheme in current GCMs. To be

579   useful for parameterization design, it is necessary for the overlap behavior we observe

580   to be related to quantities predicted by a GCM. In view of the cloud types are

581   governed by different types of atmospheric motion and state, we thus consider

582   environmental conditions related to cloud formation as a means to parameterize the

583   overlap characteristics in numerical models. But, before that, statistical connection

584   between multilayered cloud types and the environmental conditions should be

585   established in the future studies by using global cloud-overlap and meteorological

586   reanalysis datasets.

587   The global distributions and statistical results of the cumulative relative difference

588   and the cumulative overlap parameter for all multilayered cloud types are shown in

589   Fig. 9 and Tables 3 and 4, respectively. Fig. 9a shows the cumulative relative

590   difference, whereas Fig. 9b shows the cumulative overlap parameter. In Fig. 9a, we

591   find that the cloud fractions based on the random overlap assumption are

592   underestimated over the vast ocean, except over the west-central Pacific Ocean warm

pool. Obvious overestimations occur over tropical and subtropical land masses, particularly where low multilayered cloud fractions are found, such as in equatorial central South America, southern and northern Africa, Australia and the Antarctic. In these regions, the High-over-Ac system is the dominant multilayered cloud type. This pattern indicates that land surface effects may favor an exponential random overlap. In Fig. 9b, the distributions of the cumulative overlap parameter are similar to the results of the cumulative relative difference. Negative overlap parameters also occur over the vast ocean, except over the west-central Pacific Ocean warm pool. The typical negative high-value centers correspond to the major Sc-dominated oceanic areas very well. The positive overlap parameters are mostly located over tropical and subtropical land masses and Antarctica. Globally, by using random overlap, the overlap percentages are overestimated by 24%, 21.9%, 30% and 133.3% for High clouds over As, St/Sc clouds, Ns, and Ac over St/Sc clouds, respectively, over land during the daytime (Table 3). An overestimation also occurs for As over Cu and St/Sc clouds. However, the overlap of High clouds with Ac and Cu is underestimated by -32.6% and -25% over land during the daytime, respectively. Regardless of vertical separation of two types, the absolute errors of cloud-type fractions (See Tables 3 and 4) seem small for global mean, but we should recall the previous finding that a 4% increase in low cloud cover would be sufficient to offset the warming effect of a doubling of CO_2 (Randall et al. 1984), therefore, these bias errors in cloud cover possible induce a substantial bias error in the regional radiation budget. The underestimations (or overestimations) of the cloud fraction by the random overlap assumption ultimately cause overestimations (or underestimations) of cloud radiative effects. Globally, the overestimations of the net cloud radiative effect are obvious for High+St/Sc and Ac+St/Sc (approximately 3.9 W/m^2 at the surface, about 3.3% of the mean cloud forcing), whereas the underestimations of the net cloud radiative effect are obvious for High+Ac and High+Cu (Table 3). Generally speaking, change in cloud forcing caused by these bias errors in cloud cover is about 11 W/m^2 at the surface, about 10% of the mean cloud radiative effect at the surface. Thus, if these bias errors in cloud cover codified in GCMs, could bias climate feedbacks resulting

623 from increasing trace gasses or natural variability.

5. Summary and discussion

625   Although cloud types and their co-occurrence variations are the most significant

626 components of the global climate system and cloud climatology studies, systematic

627 and global studies on statistical properties of clouds have not received much attention.

628 This study quantitatively evaluates the co-occurrence frequencies of different cloud

629 types, analyzes their along-track horizontal scales and radiative effects by using the

630 latest cloud classification (2B-CLDCLASS-Lidar) and radiative flux products

631 (2B-FLXHR-LIDAR) based on 4 years of combined measurements from CALIPSO

632 and CloudSat. We also preliminary evaluate cloud-overlap assumptions. Although

633 some statistical results reasonably agree with previous research, new insights are also

634 achieved in this paper.

635   The statistical results clearly show that High clouds, As, Ac and Cu tend to

636 co-exist with other cloud types. However, St/Sc, Ns and convective clouds are much

637 more likely to exhibit individual features than other cloud types. The zonal variations

638 in along-track horizontal scales are distinct for different multilayered cloud systems.

639 On average over the globe, As+St/Sc has a maximum scale (17.4 km) and STD (23.5

640 km), while Ac+Cu has a minimum scale (2.8 km) and STD (3.1 km). By considering

641 the weight of each multilayered cloud type, the global mean instantaneous net cloud

642 radiative effects of all multilayered cloud systems during the daytime are

643 approximately -41.3 W/m^2 and -50.2 W/m^2, which account for 40.1% and 42.3% of

644 the global mean total net CREs at the top of the atmosphere (TOA) and at the surface,

645 respectively. However, the net radiative effects of ten multilayered cloud types in our

646 study are -22.7 W/m^2 and -27.1 W/m^2 (a radiative contribution of 22%) at the TOA

647 and at the surface, respectively. High+Ac and High+Sc/St (or Cu) cloud systems

648 dominate the weighted global mean net CREs of multilayered cloud types because

649 they are most frequent.

650   Active sensors allow us to preliminarily evaluate how well the overlap

651 assumptions describe the actual overlap of two separate cloud types. In summary, the

652 cloud fractions based on the random overlap assumption are mainly underestimated

653 over the vast ocean, except over the west-central Pacific Ocean warm pool. Obvious

654 overestimations occur over tropical and subtropical land masses, particularly in

655 regions with low multilayered cloud fractions. These bias errors in cloud cover may

656 induce a substantial bias error in the regional radiation budget. Globally, change in

657 cloud forcing caused by these bias errors is about 11 W/m^2 at the surface, contributes

658 an about 10% of the mean cloud radiative effect at the surface. Considering that

659 negative overlap parameters occur over the vast ocean, particularly poleward of 40 °S,

660 we suggest that a linear combination of minimum and random overlap assumptions

661 may further improve the predictions of actual cloud fractions for multilayered cloud

662 types (e.g., As+St/Sc and Ac+St/Sc) over the Southern Ocean. In fact, negative

663 overlap parameters indicate that fractions of cloud overlap are overestimated by

664 random overlap assumption at mid and high latitudes of two hemispheres, and a

665 tendency for an even more minimal degree of overlap than that predicted by the

666 random overlap assumption is exist over there. Due to passive sensors (such as,

667 ISCCP) usually fail to detect effectively the cloud overlap, thus minimum overlap is

668 what ISCCP or another passive sensor would observe. However, why do the active

669 sensors in our results and previous studies (Hogan and Illingworth, 2000; Mace et al.,

670 2002) also tend into this direction over those regions? The reason possible is as cloud

671 features in one bigger grid box (here, 2 °×2 °) associated with vertical wind shears (or

672 other dynamical factors in those regions) that are sloped in space to become more

673 grouped together, thus trending toward increasing cloud cover over there. But, similar

674 trend whether can be observed by active sensors in a smaller spatial scale (such as,

675 1 °×1 °) still needs to be confirmed in the future study by using this dataset. Generally

676 speaking, this study further verifies that factors such as dynamics related to cloud

677 formation could be connected to the way cloudy layers overlap. Therefore, we may

678 consider environmental conditions as a means to parameterize the overlap

679 characteristics in order to be useful for parameterization design in numerical models.

680 In addition, the seasonal variations of cloud overlap also must be studied, as one

681 would expect if cloud systems are driven by processes related to convection during

682 the warm season and synoptic scale systems during winter (Mace et al., 2002).

683   Previous studies have quantitatively evaluated the global mean cloud fraction of

684   each cloud type using various datasets (such as ISCCP). However, we identify new

685   features that were not observed with the ISCCP D1 dataset (Doutriaux-Boucher and

686   Seze, 1998). For example, As and Ac prevail over the arid/semi-arid land of the

687   Northern Hemisphere (northwestern China and North America) and Southern

688   Hemisphere (Australia and southern Africa), respectively. Although the

689   representations and simulations of these mid-level clouds in global climate models are

690   poor and under-predicted (Zhang et al., 2005), the balance of phases for these

691   mixed-phase clouds (mid-level clouds) due to cloud-layer temperature or ice nuclei

692   (IN) changes will certainly have a potentially large radiative impact in local regions

693   (Sassen and Khvorostyanov, 2007). Thus, to quantify the feedback of an individual

694   cloud type in these regions and document the local cloud climatology, related studies

695   on mid-level clouds in these arid/semi-arid regions should focus on the impacts of

696   dust aerosols on radiative effects and "cold rain processes" (Huang et al., 2006c;

697   2006d; Su et al., 2008; Wang et al., 2010).

698

707

708   **References**

709   Ackerman, T. P., Liou, K.N., Valero, F. P. J., and Pfister, L.: Heating rates in tropical

710   anvils, J. Atmos. Sci., 45, 1606–1623, 1988.

711   Barker, H.W.: Overlap of fractional cloud for radiation calculations in GCMs: a

712   global analysis using CloudSat and CALIPSO data, J. Geophys. Res., 113,

713 D00A01, doi:10.1029/2007JD009677, 2008.

Baum, B. A. and Wielicki, B. A.: Cirrus Cloud Retrieval Using Infrared Sounding Data: Multilevel Cloud Errors, J. Appl. Meteor., 33, 107–117, 1994.

Behrangi, A., Kubar, T., and Lambrigtsen, B. H.: Phenomenological Description of Tropical Clouds Using CloudSat Cloud Classification, Mon. Weather. Rev., 140, 3235–3249, 2012.

Betts, A. K. and Boers, R.: A cloudiness transition in a marine boundary layer, J. Atmos. Sci., 47, 1480–1497, 1990.

Cess, R. D., Potter, G. L., Blanchet, J. P., Boer, G. J., Del Genio, A. D., Déqué, M., Dymnikov, V., Galin, V., Gates, W. L., Ghan, S. J., Kiehl, J. T., Lacis, A. A., Le Treut, H., Li, Z. X., Liang, X.Z., McAvaney, B. J., Meleshko, V. P., Mitchell, J. F. B., Morcrette, J. J., Randall, D. A., Rikus, L., Roeckner, E., Royer, J. F., Schlese, U., Sheinin, D. A., Slingo, A., Sokolov, A. P., Taylor, K.E., Washington, W. M., Wetherald, R. T., Yagai, I., and Zhang, M. H.: Intercomparison and interpretation of climate feedback processes in 19 atmospheric general circulation models, J. Geophys. Res., 95, 16601–16615, 1990.

Chang, F. L. and Li, Z.: A new method for detection of cirrus overlapping- low clouds and determination of their optical properties, J. Atmos. Sci., 62, 3993–4009, 2005a.

Chang, F. L. and Li, Z.: A near global climatology of single-layer and overlapped clouds and their optical properties retrieved from TERRA/MODIS data using a new algorithm, J. Clim., 18, 4752–4771, 2005b.

Chen, B., Huang, J., Minnis, P., Hu, Y., Yi, Y., Liu, Z., Zhang, D., and Wang, X.: Detection of dust aerosol by combining CALIPSO active lidar and passive IIR measurements, Atmos. Chem. Phys., 10, 4241-4251, 2010.

Chen, C. and Cotton, W. R.: The physics of the marine stratocumulus- capped mixed layer, J. Atmos. Sci., 44, 2951–2977, 1987.

Chen, T., Rossow, W. B., and Zhang, Y.: Radiative Effects of Cloud-Type Variations, J. Clim., 13, 264–286, 2000.

Choi, Y.S., Lindzen, R.S., Ho, C.H., and Kim, J.: Space observations of cold-cloud

743 phase change, Proc. Natl Acad. Sci., 107, 11211–11216, 2010.

744 Doutriaux-Boucher, M. and Seze, G.: Significant changes between the ISCCP C and D
745 cloud climatologies, Geophys. Res. Lett., 25, 4193-4196, 1998.

746 Eastman, R. and Warren, S. G.: A 39-Yr Survey of Cloud Changes from Land Stations
747 Worldwide 1971–2009: Long-Term Trends, Relation to Aerosols, and Expansion
748 of the Tropical Belt, J. Clim., 26, 1286-1303, 2013.

749 Eastman, R., Warren, S. G., and Hahn, C. J.: Variations in Cloud Cover and Cloud
750 Types over the Ocean from Surface Observations, 1954–2008, J. Clim., 24,
751 5914–5934, doi: 10.1175/2011JCLI3972.1, 2011.

752 Hagihara, Y., Okamoto, H., and Yoshida, R.: Development of a combined
753 CloudSat/CALIPSO cloud mask to show global cloud distribution, J. Geophys.
754 Res., 115, D00H33, doi:10.1029/2009JD012344, 2010.

755 Hahn, C. J., Rossow, W. B., and Warren, S. G.: ISCCP Cloud Properties Associated
756 with Standard Cloud Types Identified in Individual Surface Observations, J.
757 Clim., 14, 11–28, 2001.

758 Han, Q., Rossow, W. B., and Lacis, A. A.: Near-global survey of effective droplet
759 radii in liquid water clouds using ISCCP data, J. Clim., 7, 465-497, 1994.

760 Hartmann, D. L., Ockert-Bell, M. E., and Michelsen, M.L.: The effect of cloud type
761 on Earth's energy balance: global analysis, J. Clim., 5, 1281–1304, 1992.

762 Haynes, J.M., Jakob, C., Rossow, W.B., Tselioudis, G., and Brown, J.: Major
763 Characteristics of Southern Ocean Cloud Regimes and Their Effects on the
764 Energy Budget, J. Clim., 24, 5061-5080. doi: 10.1175/2011JCLI4052.1, 2011.

765 Haynes, J.M., Vonder-Haar, T.H., L'Ecuyer, T., Henderson, D.: Radiative heating
766 characteristics of Earth's cloudy atmosphere from vertically resolved active
767 sensors, Geophys. Res. Lett., 40, 624–630, doi:10.1002/grl.50145, 2013.

768 Henderson, D.S., L'Ecuyer, T., Stephens, G., Partain, P., and Sekiguchi, M.: A
769 multi-sensor perspective on the radiative impacts of clouds and aerosols, J. Appl.
770 Meteorol. Climatol., 52, 853–871, doi: 10.1175/JAMC-D-12-025.1, 2013.

771 Hogan, R. J. and Illingworth, A. J.: Deriving cloud overlap statistics from radar, Q. J.
772 Roy. Meteor. Soc., 128, 2903–2909, 2000.

773 Huang, J.P.: Analysis of ice water path retrieval errors over tropical ocean,
774   Advances in Atmospheric Sciences, 23: 165-180, 2006a.

775 Huang, J. P., Minnis, P., and Lin, B.: Advanced retrievals of multilayered cloud
776   properties using multispectral measurements, J. Geophys. Res., 110, D15S18,
777   doi:10.1029/2004JD005101, 2005.

778 Huang, J. P., Minnis, P., and Lin, B.: Determination of ice water path in ice-
779   over-water cloud systems using combined MODIS and AMSR-E measurements,
780   Geophys. Res. Lett., 33, L21801, doi:10.1029/ 2006GL027038, 2006b.

781 Huang, J.P., Lin, B., Minnis, P., Wang, T., Wang, X., Hu, Y., Yi, Y., and Ayers, J.R.:
782   Satellite-based assessment of possible dust aerosols semi-direct effect on cloud
783   water path over East Asia, Geophys. Res. Lett., 33, L19802, doi:
784   10.1029/2006GL026561, 2006c.

785 Huang, J.P., Minnis, P., Lin, B., Wang, T., Yi, Y., Hu, Y., Sun-Mack, S., and Ayers,
786   K.: Possible influences of Asian dust aerosols on cloud properties and radiative
787   forcing observed from MODIS and CERES, Geophys. Res. Lett., 33, L06824,
788   doi: 10.1029/2005GL024724, 2006d.

789 Kato, S., Sun-Mack, S., Miller, W. F., Rose, F. G., Chen, Y., Minnis, P., and Wielicki,
790   B. A.: Relationships among cloud occurrence frequency, overlap, and effective
791   thickness derived from CALIPSO and CloudSat merged cloud vertical profiles, J.
792   Geophys. Res., 115, D00H28, doi:10.1029/2009JD012277, 2010.

793 Klein, S. A. and Hartmann, D. L.: The seasonal cycle of low stratiform clouds, J.
794   Clim., 6, 1588–1606, 1993.

795 L'Ecuyer, T.S., Wood, N., Haladay, T., and Stephens, G.L.: The impact of clouds on
796   atmospheric heating based on the R04 CloudSat fluxes and heating rate dataset, J.
797   Geophys. Res., 113, D00A15, doi:10.1029/2008JD009951, 2008.

798 Li, J., Yi, Y., Minnis, P., Huang, J., Yan, H., Ma, Y., Wang, W., and Ayers, k.:
799   Radiative effect differences between multi-layered and single-layer clouds
800   derived from CERES, CALIPSO, and CloudSat data, J. Quant. Spectrosc. Radiat.
801   Transf., 112, 361–375, 2011.

802 Liang, X.Z., and Wu, X.: Evaluation of a GCM subgrid cloudradiation interaction

803   parameterization using cloud-resolving model simulations, Geophys. Res. Lett.,

804   32, L06801, doi:10.1029/2004 GL022301, 2005.

805 Liao, X., Rossow, W. B., and Rind, D.: Comparison between SAGE II and ISCCP

806   high-level clouds. Part I: Global and zonal mean cloud amounts, J. Geophys.

807   Res., 100, 1121–1135, 1995.

808 Luo, Y., Zhang, R., and Wang, H.: Comparing occurrences and vertical structures of

809   hydrometeors between the eastern China and the Indian monsoon region using

810   CloudSat/CALIPSO data, J. Clim., 22, 1052-1064, 2009.

811 Mace, G. G., and Benson-Troth, S.: Cloud-layer overlap characteristics derived from

812   long-term cloud radar data, J. Clim., 15, 2505–2515, 2002.

813 Minnis, P., Yi, Y., Huang, J., and Ayers, J. K.: Relationships between radiosonde and

814   RUC-2 meteorological conditions and cloud occurrence determined from ARM

815   data, J. Geophys. Res., 110, D23204, doi:10.1029/2005JD006005, 2005.

816 Minnis, P., Huang, J., Lin, B., Yi, Y., Arduim, R., Fan, T.-F., Ayers, J. K., and Mace,

817   G. G.: Ice cloud properties in ice-over-water cloud systems using Tropical

818   Rainfall Measuring Mission (TRMM) visible and infrared scanner and TRMM

819   Microwave Imager data, J. Geophys. Res., 112, D06206, doi:

820   10.1029/2006JD007626, 2007.

821 Moran, J.M., Morgan, M.D., and Pauley, P.M.: *Meteorology: The Atmosphere and the*

822   *Science of Weather*, Prentice Hall, New Jersey, 530pp, 1997.

823 Morcrette, J. J. and Jakob, C.: The response of the ECMWF model to changes in the

824   cloud overlap assumption, Mon. Weather. Rev., 128, 1707–1732, 2000.

825 Naud, C.M., DelGenio, A.D., Mace, G.G., Benson, S., Clothiaux, E.E., and Kollias, P.:

826   Impact of dynamics and atmospheric state on cloud vertical overlap, J. Clim., 21,

827   1758–1770, 2008.

828 Norris, J. R. and Leovy, C. B.: Interannual variability in stratiform cloudiness and sea

829   surface temperature, J. Clim., 7, 1915–1925, 1994.

830 Parker, S.P.: *Meteorology Source Book*. McGraw-Hill, New York, 304 pp, 1988.

831 Randall, D.A., Coakley, Jr. J.A., Fairall, C.W., Kropfli, R.A., and Lenschow, D.H.:

832   Outlook for research on sub-tropical marine stratiform clouds, Bull. Amer.

Meteorol. Soc., 65, 1290–1301, 1984.

Rossow, W. B. and Schiffer, R. A.: ISCCP cloud data products, B. Am. Meteorol. Soc., 72, 2–20, 1991.

Rossow, W. B. and Schiffer, R. A.: Advances in understanding clouds from ISCCP, B. Am. Meteorol. Soc., 80, 2261– 2286, 1999.

Sassen, K. and Cho, B. S.: Subvisual–thin cirrus lidar dataset for satellite verification and climatological research, J. Appl. Meteor., 31, 1275–1285, 1992.

Sassen, K., and Khvorostyanov, V.I.: Microphysical and radiative properties of mixed phase altocumulus: a model evaluation of glaciation effects. Atmos. Res., 84, 390–398, 2007.

Sassen, K. and Wang, Z.: Classifying clouds around the globe with the CloudSat radar: 1-year of results, Geophys. Res. Lett., 35, L04805, doi:10.1029/2007GL032591, 2008.

Sassen, K., Wang, Z., and Liu, D.: Cirrus clouds and deep convection in the tropics: Insights from CALIPSO and CloudSat, J. Geophys. Res., 114, D00H06, doi:10.1029/2009JD011916, 2009.

Stephens, G. L.: Cloud feedbacks in the climate system: a critical review, J. Clim., 18, 237–273, 2005.

Stephens, G. L., Wood, N. B., and Gabriel, P. M.: An assessment of the parameterization of subgrid-scale cloud effects on radiative transfer: Part I. Vertical overlap, J. Atmos. Sci., 61, 715–732, 2004.

Stephens, G.L., Vane, D.G., Boain, R.J., Mace, G.G., Sassen, K., Wang, Z., Illingworth, A.J., O'Connor, E.J., Rossow, W.B., Durden, S.L., Miller, S.D., Austin, R.T., Benedetti, A., Mitrescu, C., and CloudSat Science Team.: The CloudSat mission and the A-Train, A new dimension of space-based observations of clouds and precipitation, B. Am. Meteorol. Soc., 83, 1771–1790, 2002.

Su, J., Huang, J., Fu, Q., Minnis, P., Ge, J., and Bi, J.: Estimation of Asian dust aerosol effect on cloud radiation forcing using Fu-Liou radiative model and CERES measurements, Atmos. Chem. Phys., 8, 2763-2771, 2008.

863   Tian, L. and Curry, J. A.: Cloud overlap statistics, J. Geophys. Res., 94, 9925−9935,
864   1989.

865   Trenberth, K.E., and Fasullo, J.T.: Simulation of present-day and twenty-first-century
866   energy budgets of the southern oceans, J. Clim., 23, 440–454, 2010.

867   Wang, L. and Dessler, A. E.: Instantaneous cloud overlap statistics in the tropical area
868   revealed by ICESat/GLAS data, Geophys. Res. Lett., 33, L15804,
869   doi:10.1029/2005GL024350, 2006.

870   Wang, Z. and Sassen, K.: Cloud type and macrophysical property retrieval using
871   multiple remote sensors, J. Appl. Meteor., 40, 1665–1682, 2001.

872   Wang, W., Huang, J., Minnis, P., Hu, Y., Li, J., Huang, Z., Ayers, J. K., and Wang, T.:
873   Dusty cloud properties and radiative forcing over dust source and downwind
874   regions derived from A-Train data during the Pacific Dust Experiment, J.
875   Geophys. Res., 115, D00H35, doi: 10.1029/2010JD014109, 2010.

876   Warren, S. G., Eastman, R. M., and Hahn, C. J.: A survey of changes in cloud cover
877   and cloud types over land from surface observations, 1971–96, J. Clim., 20,
878   717–738, 2007.

879   Warren, S. G., Hahn, C. J., and London, J.: Simultaneous occurrence of different cloud
880   types, J. Clim. Appl. Meteorol., 24, 658–67, 1985.

881   Winker D. M., Hunt, W. H., and Mcgill, M. J.: Initial performance assessment of
882   CALIOP, Geophys. Res. Lett., 34, L19803, doi:10.1029/ 2007GL030135, 2007.

883   World Meteorological Organization.: *International Cloud Atlas: Abridged atlas*,
884   World Meteorological Organization, 62 pp., and 72 plates, Geneva, 1956.

885   Wylie, D.P., Eloranta, E., Spinhirne, J.D., and Palm, S.P.: A comparison of cloud
886   cover statistics from the GLAS lidar with HIRS, J. Clim., 20, 4968–4981,
887   doi:10.1175/JCLI4269.1, 2007.

888   Yu, R. C., Wang, B., and Zhou, T.: Climate effects of the deep continental stratus
889   clouds generated by the Tibetan Plateau, J. Clim., 17, 2702-2713, 2004.

890   Yu, H., Remer, L. A., Chin, M., Bian, H., Tan, Q., Yuan, T., and Zhang, Y.: Aerosols
891   from overseas rival domestic emissions over North America, Science, 337(6094),
892   566–569, doi:10.1126/science.1217576, 2012.

893 Yuan, T. and Oreopoulos, L.: On the global character of overlap between low and
894   high clouds, Geophys. Res. Lett., 40, 5320–5326, doi:10.1002/grl.50871, 2013.

895 Zhang, D., Luo, T., Liu, D., and Wang, Z.: Spatial Scales of Altocumulus Clouds
896   Observed with Collocated CALIPSO and CloudSat Measurements, Atmos. Res.,
897   148, 58-69, doi: 10.1016/j.atmosres.2014.05.023, 2014.

898 Zhang, M. H., Lin, W. Y., Klein, S. A., Bacmeister, J. T., Bony, S., Cederwall, R. T.,
899   Del Genio, A.D., Hack, J. J., Loeb, N. G., Lohmann, U., Minnis, P., Musat, I.,
900   Pincus, R., Stier, P., Suarez,M. J., Webb, M. J., Wu, J. B., Xie, S. C., Yao, M. S.,
901   and Zhang, J. H.: Comparing clouds and 15 their seasonal variations in 10
902   atmospheric general circulation models with satellite measurements, J. Geophys.
903   Res., 110, D15S02, doi:10.1029/2004JD005021, 2005.

904

905

906

907

908

909

910

911

912

913

914

915

916

917

918

919

920

921

922

923

924

Table 1. Globally averaged overlapping percentages of different cloud types over land and ocean during daytime.

	SL[a]	ML[b]	High	As	Ac	St/Sc	Cu	Ns	Deep	surface
High	8.8	14.5	3.7	2.5	4.3	3.2	2.8	1.0	0.4	Land
	8.8	**16.4**	**4.1**	**2.2**	**3.5**	**5.2**	**3.5**	**1.2**	**0.3**	**Ocean**
As	6.5	6.7	--	0.9	1.0	2.0	1.1	0.4	--	Land
	4.2	**6.1**	**--**	**0.5**	**0.9**	**2.5**	**1.0**	**0.3**	**--**	**Ocean**
Ac	5.3	7.0	--	0.01	1.1	0.9	1.1	0.04	--	Land
	3.1	**6.4**	**--**	**0.01**	**0.8**	**1.5**	**1.0**	**0.08**	**--**	**Ocean**
St/Sc	10.5	6.2	--	--	--	0.3	0.5	--	--	Land
	21.9	**9.4**	**--**	**--**	**--**	**0.4**	**0.7**	**--**	**--**	**Ocean**
Cu	3.9	5.1	--	--	--	0.1	0.3	--	--	Land
	6.6	**5.9**	**--**	**--**	**--**	**0.2**	**0.3**	**--**	**--**	**Ocean**
Ns	4.0	1.5	--	--	--	0.02	0.09	--	--	Land
	4.1	**1.6**	**--**	**--**	**--**	**0.02**	**0.05**	**--**	**--**	**Ocean**
Deep	0.8	0.4	--	--	--	--	--	--	--	Land
	0.8	**0.3**	**--**	**--**	**--**	**--**	**--**	**--**	**--**	**Ocean**

[a]The SL represents the single-layered cloud. [b]The ML represents the multi-layered cloud. And, those boldfaced values indicated the overlapping percentages of different cloud types over ocean.

929

Table 2. Globally averaged overlapping percentages for different cloud types over land and ocean during nighttime.

	SL[a]	ML[b]	High	As	Ac	St/Sc	Cu	Ns	Deep	surface
High	12.0	17.4	5.5	3.2	6.6	2.6	1.8	1.3	0.3	Land
	8.8	**20.8**	**4.7**	**2.3**	**5.0**	**7.6**	**4.4**	**1.3**	**0.3**	**Ocean**
As	6.9	7.4	--	1.0	1.1	1.9	0.9	0.4	--	Land
	3.9	**6.3**	**--**	**0.4**	**0.9**	**2.6**	**1.0**	**0.3**	**--**	**Ocean**
Ac	4.6	8.5	--	0.01	1.2	0.7	0.6	0.05	--	Land
	3.1	**8.1**	**--**	**0.01**	**1.0**	**1.9**	**1.2**	**0.08**	**--**	**Ocean**
St/Sc	6.4	5.1	--	--	--	0.2	0.3	--	--	Land
	23.8	**12.1**	**--**	**--**	**--**	**0.4**	**0.8**	**--**	**--**	**Ocean**
Cu	2.0	3.4	--	--	--	0.1	0.2	--	--	Land
	5.9	**6.9**	**--**	**--**	**--**	**0.2**	**0.4**	**--**	**--**	**Ocean**
Ns	3.9	1.7	--	--	--	--	0.08	--	--	Land
	4.0	**1.7**	**--**	**--**	**--**	**--**	**0.05**	**--**	**--**	**Ocean**
Deep	0.8	0.3	--	--	--	--	--	--	--	Land
	0.9	**0.3**	**--**	**--**	**--**	**--**	**--**	**--**	**--**	**Ocean**

[a]The SL represents the single-layered cloud. [b]The ML represents the multi-layered cloud. And, those boldfaced values indicated the overlapping percentages of different cloud types over ocean.

934

935

Table 3. Cloud fractions of different multilayered cloud types based on different overlap assumptions and observations during daytime. Here, $C_{overlap}$ and $C_1 \times C_2$ are the overlap cloud fraction from observations and overlap assumptions. "*a*" presents the overlap parameter.

Cloud type	C_{max}	C_{random}	C_{real}	$C_1 \times C_2$	$C_{overlap}$	R^a (W/m^2)	Diff.[b]	*a*
High+As	23.3	33.4	34.0	3.1	2.5	0.8	24.0%	-0.06
	(25.2)	**(32.9)**	**(33.3)**	**(2.6)**	**(2.2)**	**(0.8)**	**(18.2%)**	**(-0.05)**
High+Ac	23.3	32.7	31.3	2.9	4.3	-2.4	-32.6%	0.15
	(25.2)	**(32.3)**	**(31.2)**	**(2.4)**	**(3.5)**	**(-2.3)**	**(-31.4%)**	**(0.15)**
High+St/Sc	23.3	36.1	36.8	3.9	3.2	1.0	21.9%	-0.05
	(31.3)	**(48.6)**	**(51.3)**	**(7.9)**	**(5.2)**	**(3.9)**	**(51.9%)**	**(-0.16)**
High+Cu	23.3	30.2	29.5	2.1	2.8	-1.3	-25.0%	0.1
	(25.2)	**(34.5)**	**(34.2)**	**(3.2)**	**(3.5)**	**(-0.7)**	**(-8.6%)**	**(0.03)**
High+Ns	23.3	27.5	27.8	1.3	1.0	0.7	30.0%	-0.07
	(25.2)	**(29.5)**	**(29.7)**	**(1.4)**	**(1.2)**	**(0.5)**	**(16.7%)**	**(-0.05)**
High+Deep	23.3	24.2	24.1	0.3	0.4	-0.1	-25.0%	0.11
	(25.2)	**(26.0)**	**(26.0)**	**(0.3)**	**(0.3)**	**(0.0)**	**(0.0%)**	**(0.0)**
As+St/Sc	16.7	27.7	27.9	2.2	2.0	0.6	10.0%	-0.02
	(31.3)	**(38.4)**	**(39.1)**	**(3.2)**	**(2.5)**	**(2.5)**	**(28.0%)**	**(-0.1)**
As+Cu	13.2	21.0	21.1	1.2	1.1	0.4	9.1%	-0.01
	(12.5)	**(21.5)**	**(21.8)**	**(1.3)**	**(1.0)**	**(1.7)**	**(30.0%)**	**(-0.03)**
Ac+St/Sc	16.7	26.9	28.1	2.1	0.9	2.2	133.3%	-0.12
	(31.3)	**(37.8)**	**(39.3)**	**(3.0)**	**(1.5)**	**(3.9)**	**(100.0%)**	**(-0.23)**
Ac+Cu	12.3	20.2	20.2	1.1	1.1	0.0	0.0%	0.0
	(12.5)	**(20.8)**	**(21.0)**	**(1.2)**	**(1.0)**	**(0.5)**	**(20.0%)**	**(-0.02)**

940 [a]Calculated from (C_{random}-C_{real})$\times$(global mean net cloud radiative effect of each cloud type). [b]Calculated from ($C_1 \times C_2$-$C_{overlap}$)/ $C_{overlap}$.

941 And, those boldfaced values in the brackets indicated the overlapping percentages of different cloud types over ocean surface. But for R^a,

942 the values indicated the net cloud radiative effect difference between real and random overlap at TOA and Surface (in the brackets),

943 respectively. Here, only cloud radiative effects during daytime are considered.

944
945
946
947
948
949
950
951
952
953
954
955
956
957

958

959 Table 4. Cloud fractions of different multilayered cloud types based on different
960 overlap assumptions and observations during nighttime. Here, $C_{overlap}$ and $C_1 \times C_2$ are
961 the overlap cloud fraction from observations and overlap assumptions. "*a*" presents
962 the overlap parameter.

Cloud type	C_{max}	C_{random}	C_{real}	$C_1 \times C_2$	$C_{overlap}$	R^a(W/m^2)	Diff.[b]	*a*
High+As	29.4	39.5	40.5	4.2	3.2	-	31.3%	-0.1
	(29.6)	**(36.8)**	**(37.5)**	**(3.0)**	**(2.3)**	**-**	**(30.4%)**	**(-0.1)**
High+Ac	29.4	38.6	35.9	3.9	6.6	-	-40.9%	0.29
	(29.6)	**(37.5)**	**(35.8)**	**(3.3)**	**(5.0)**	**-**	**(-34.0%)**	**(0.22)**
High+St/Sc	29.4	37.5	38.3	3.4	2.6	-	30.8%	-0.1
	(35.9)	**(54.9)**	**(57.9)**	**(10.6)**	**(7.6)**	**-**	**(39.5%)**	**(-0.16)**
High+Cu	29.4	33.2	33.0	1.6	1.8	-	-11.1%	0.05
	(29.6)	**(38.6)**	**(38.0)**	**(3.8)**	**(4.4)**	**-**	**(-13.6%)**	**(0.07)**
High+Ns	29.4	33.4	33.7	1.6	1.3	-	23.1%	-0.08
	(29.6)	**(33.6)**	**(34.0)**	**(1.7)**	**(1.3)**	**-**	**(30.8%)**	**(-0.1)**
High+Deep	29.4	30.2	30.2	0.3	0.3	-	0.0%	0.0
	(29.6)	**(30.4)**	**(30.5)**	**(0.4)**	**(0.3)**	**-**	**(33.3%)**	**(-0.13)**
As+St/Sc	14.3	24.2	23.9	1.6	1.9	-	-15.8%	0.03
	(35.9)	**(42.4)**	**(43.5)**	**(3.7)**	**(2.6)**	**-**	**(42.3%)**	**(-0.17)**
As+Cu	14.3	18.9	18.8	0.8	0.9	-	-11.1%	0.02
	(12.8)	**(21.7)**	**(22.0)**	**(1.3)**	**(1.0)**	**-**	**(30.0%)**	**(-0.03)**
Ac+St/Sc	13.1	23.1	23.9	1.5	0.7	-	114.3%	-0.08
	(35.9)	**(43.1)**	**(45.2)**	**(4.0)**	**(1.9)**	**-**	**(110.5%)**	**(-0.29)**
Ac+Cu	13.1	17.8	17.9	0.7	0.6	-	16.7%	-0.02
	(12.8)	**(22.6)**	**(22.8)**	**(1.4)**	**(1.2)**	**-**	**(16.7%)**	**(-0.02)**

963 [a]Calculated from (C_{random}-C_{real})×(global mean net cloud radiative effect of each cloud type).   [b]Calculated from ($C_1 \times C_2$-$C_{overlap}$)/ $C_{overlap}$.

964 And, those boldfaced values in the brackets indicated the overlapping percentages of different cloud types over ocean surface. But for R^a,

965 the values indicated the net cloud radiative effect difference between real and random overlap at TOA and Surface (in the brackets),

966 respectively. Here, only cloud radiative effects during daytime are considered.

967
968
969
970
971
972
973
974
975
976
977
978

979

980   **Figure captions**

981   Figure 1. (a) The global distribution ($2^{\circ} \times 2^{\circ}$ grid boxes) of annually averaged

982   multilayered cloud fraction. (b) The zonal distributions of seasonal averaged

983   multilayered cloud fraction.

984   Figure 2. Zonal distributions of annual most frequently occurring multilayered cloud

985   types based on the 2B-CLDCLASS-Lidar product.

986   Figure 3. The global distributions of (a) the annual mean dominant cloud types and (b)

987   the corresponding cloud fractions. And, the global distributions of (c) the annual

988   mean dominant multiple cloud types and (d) the corresponding cloud amounts.

989   Figure 4. (a)-(b):The zonal variation of cloud along-track horizontal scales for these

990   multilayered cloud systems and (c)-(d): their probability distribution.

991   Figure 5. (a)-(d):The zonal distributions of ==instantaneous net== cloud radiative effect and

992   weighted ==instantaneous net== cloud radiative effect by considering the frequency of

993   occurrence of each cloud type for different multilayered cloud systems at the top

994   of atmosphere (TOA) ==during daytime (that is, overpass time of satellite).==

995   Figure 6. Same with Figure5, but at the surface during the daytime.

996   Figure 7. The global average ==instantaneous net== cloud radiative effect and weighted

997   ==instantaneous net== cloud radiative effect for different multilayered cloud types at

998   TOA and surface only during daytime. The gray line presents the global average

999   frequency of occurrence of each cloud type only during daytime (that is, weights).

1000   The total weighted ==instantaneous net== cloud radiative effects of ten multilayered

1001   cloud system are also showed in the figure 7c and 7d. TOA (-22.7 W/m^2);

1002   Surface (-27.1 W/m^2).

1003   Figure 8. (a)-(b): ==The zonal distributions of the relative difference between the random==

1004   ==and actual overlap for different multilayered cloud types and the cumulative==

1005   ==relative difference of all multilayered cloud types (gray line).== (c)-(d): The zonal

1006   distributions of the overlap parameter for different multilayered cloud types and

1007   the cumulative overlap parameter of all multilayered cloud types (gray line).

1008   Figure 9. The global distributions of (a) the cumulative relative difference and (b) the

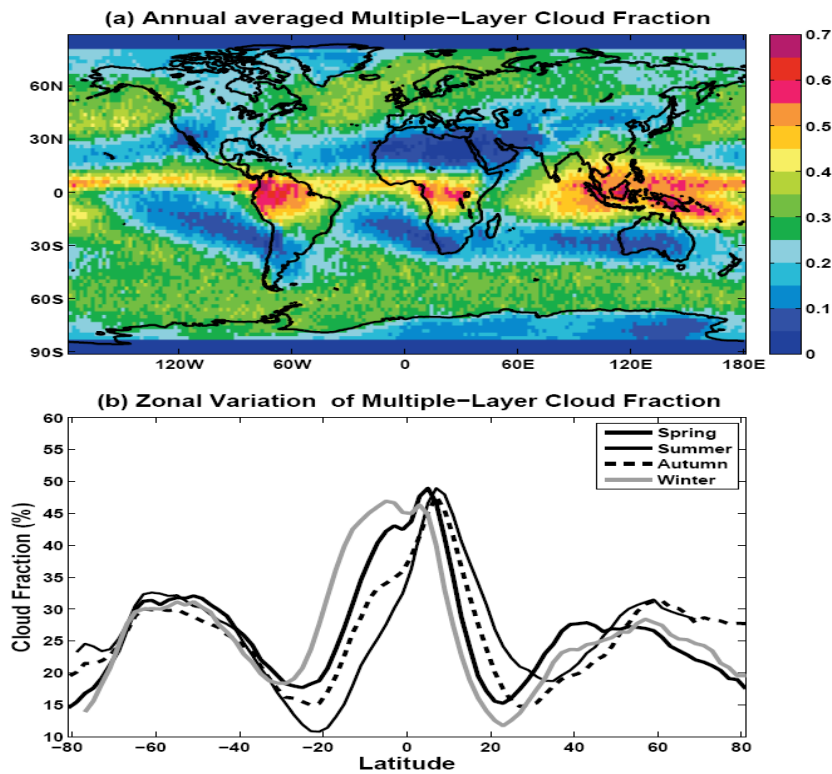cumulative overlap parameter of all multilayered cloud types.

Figure 1. (a) The global distribution ($2^{\circ} \times 2^{\circ}$ grid boxes) of annually averaged

multilayered cloud fraction. (b) The zonal distributions of seasonal averaged
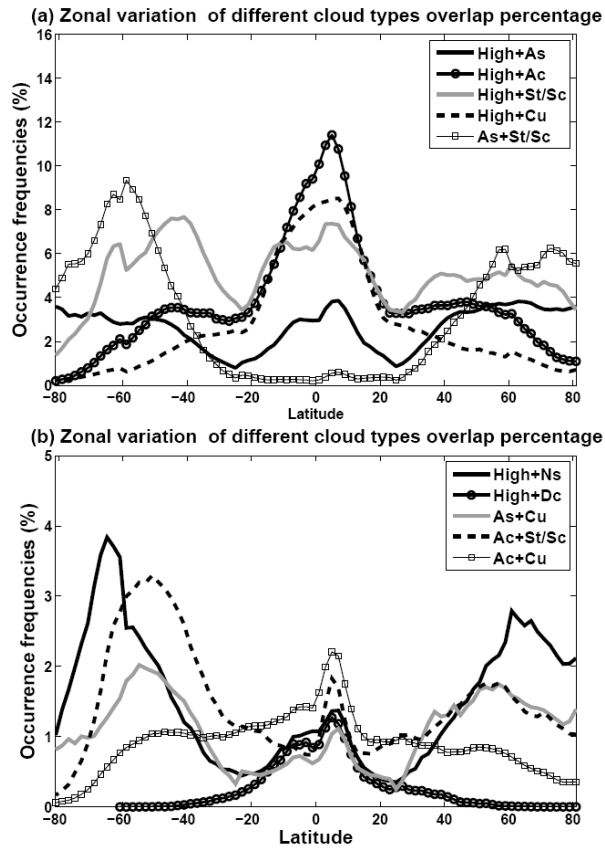
multilayered cloud fraction.

1027

1028

(a) Zonal variation of different cloud types overlap percentage

Legend:
High+As
High+Ac
High+St/Sc
High+Cu
As+St/Sc

(b) Zonal variation of different cloud types overlap percentage

Legend:
High+Ns
High+Dc
As+Cu
Ac+St/Sc
Ac+Cu

1029

1030   Figure 2. Zonal distributions of annual most frequently occurring multilayered cloud
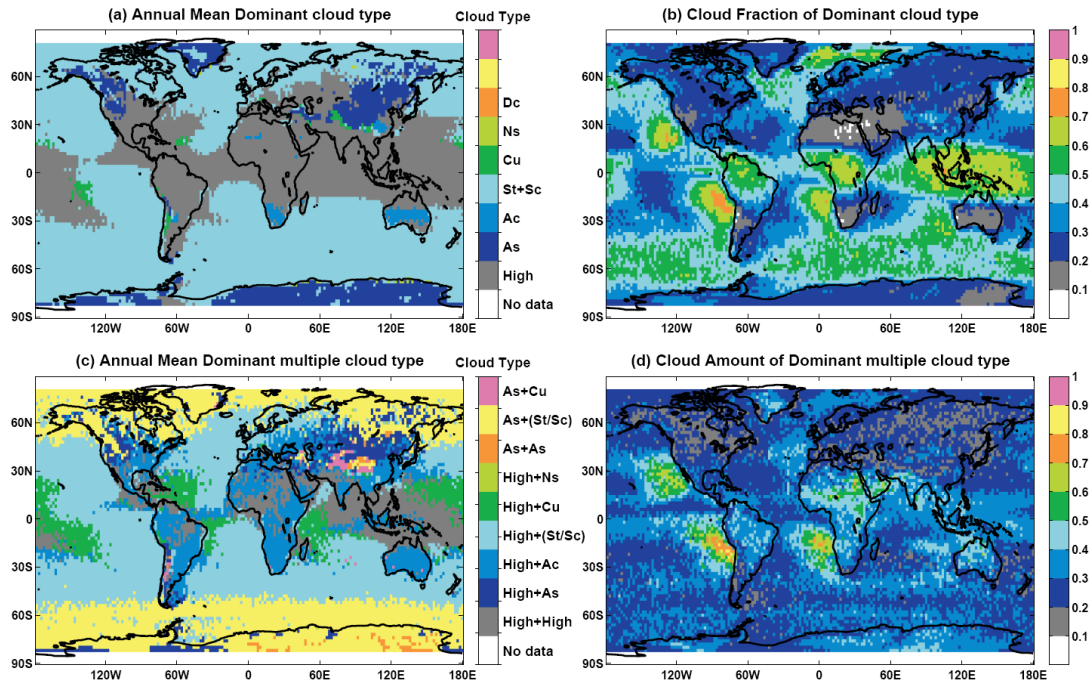
1031   types based on the 2B-CLDCLASS-Lidar product.

1032

1033

1034

1035

1036

1037

1038

1039

1040

1041

1042

1043

1044

1045

1046

1047

Figure 3. The global distributions of (a) the annual mean dominant cloud types and (b) the corresponding cloud fractions. And, the global distributions of (c) the annual mean dominant multiple cloud types and (d) the corresponding cloud amounts.
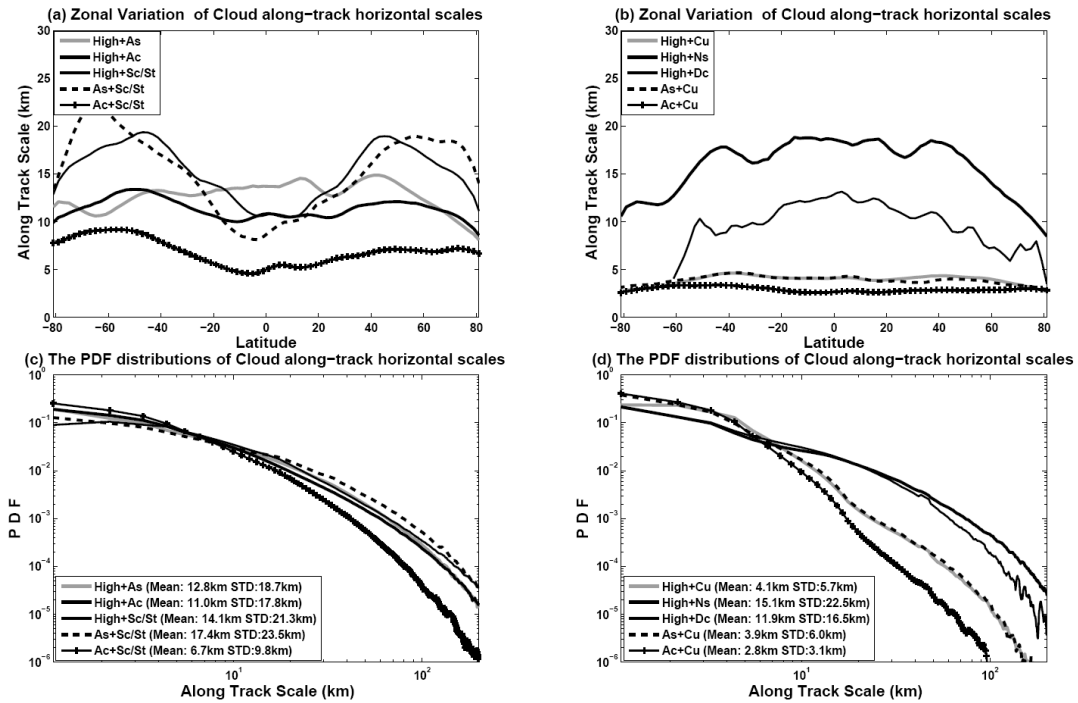
1051

1052

1053

1054

1055

1056

1057

1058

1059

1060

1061

1062

1067 Figure 4. (a)-(b):The zonal variation of cloud along-track horizontal scales for these

1068 multilayered cloud systems and (c)-(d): their probability distribution.

1069

1070

1071

1072

1073

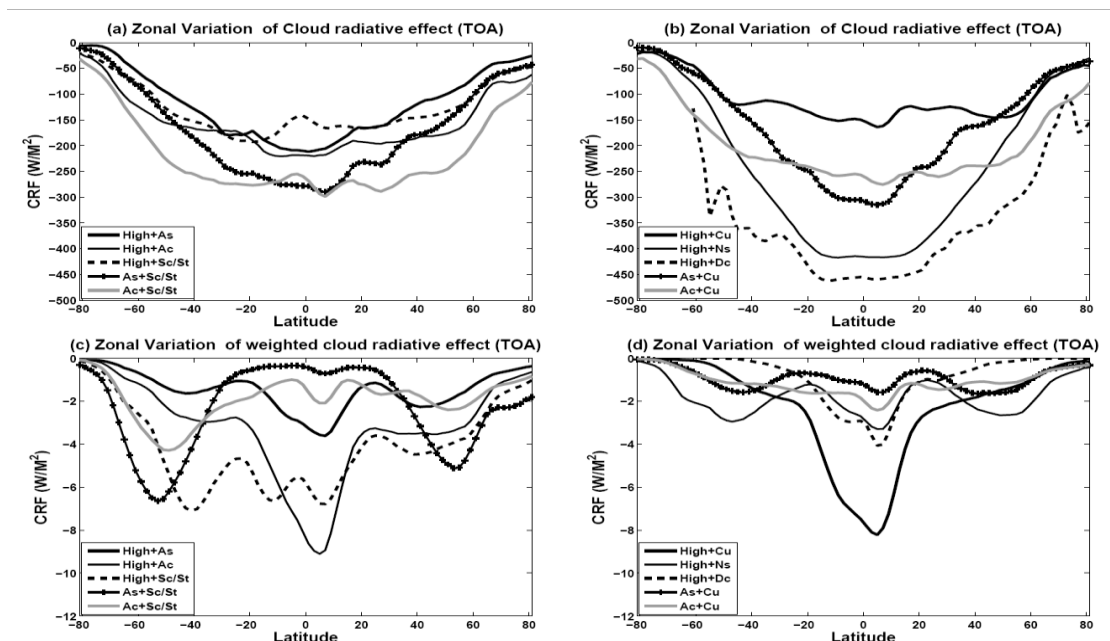1074

1075

1076

1077

1078

1079

1080

1081

1082

1083

Figure 5. (a)-(d):The zonal distributions of instantaneous net cloud radiative effect and weighted instantaneous net cloud radiative effect by considering the frequency of occurrence of each cloud type for different multilayered cloud systems at the top of atmosphere (TOA) during daytime (that is, overpass time of satellite).
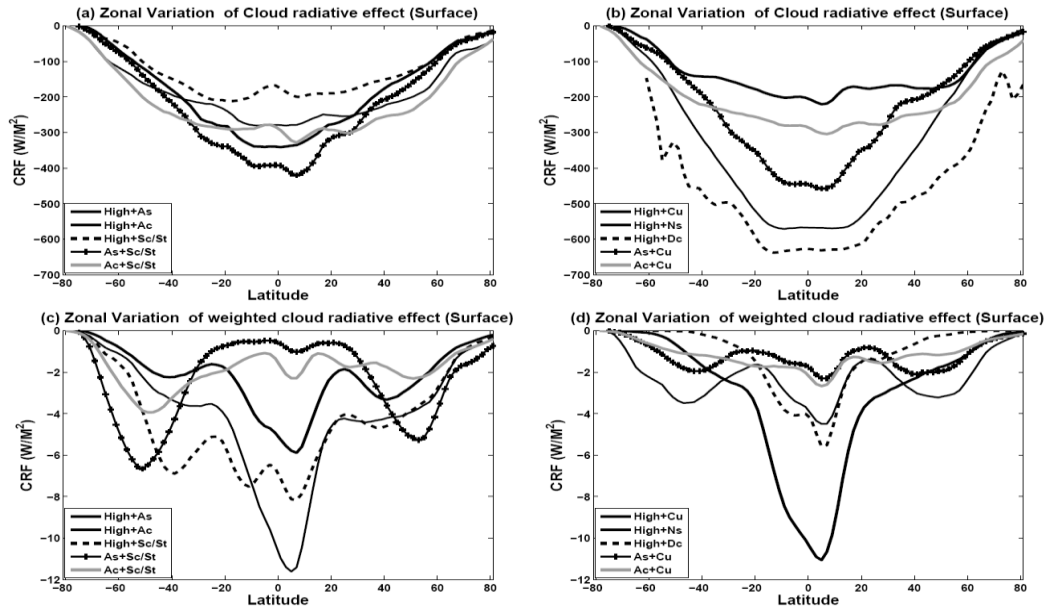
1089

1090

1091

1092

1093

1094

1095

1096

1097

1098

1099

1100

1101

1102

1103

1104

Figure 6. Same with Figure5, but at the surface during the daytime.

1105

1106

1107

1108

1109

1110

1111

1112

1113

1114

1115

1116

1117

1118
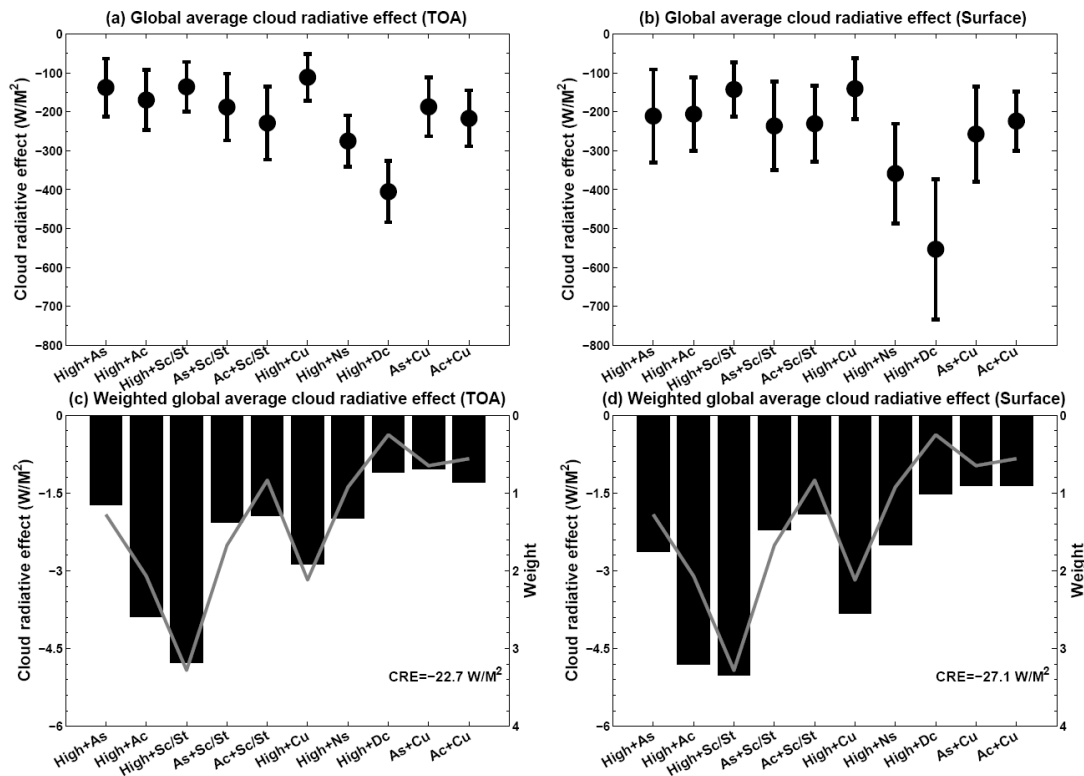
1119

1120

1121

1122

1123

1124

1125

1126

Figure 7. The global average instantaneous net cloud radiative effect and weighted
instantaneous net cloud radiative effect for different multilayered cloud types at
TOA and surface only during daytime. The gray line presents the global average
frequency of occurrence of each cloud type only during daytime (that is, weights).
The total weighted instantaneous net cloud radiative effects of ten multilayered
cloud system are also showed in the figure 7c and 7d. TOA (-22.7 W/m^2);
Surface (-27.1 W/m^2).
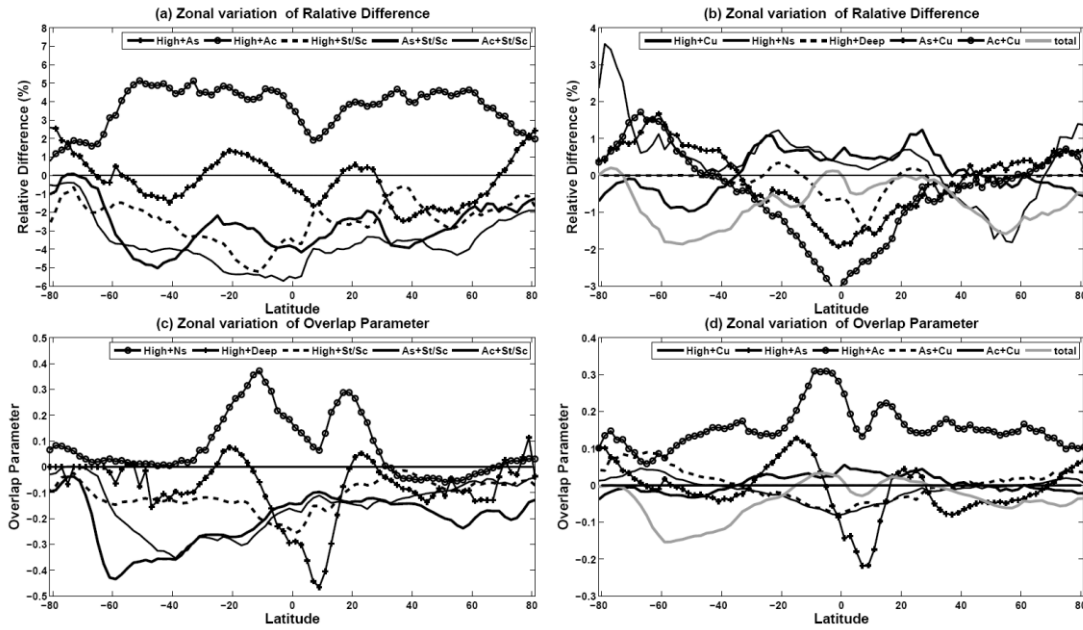
1134

1135

1136

1137

1138

1139

1140

1141

1142

Figure 8. (a)-(b): <mark>The zonal distributions of the relative difference between the random and actual overlap for different multilayered cloud types and the cumulative relative difference of all multilayered cloud types (gray line).</mark> (c)-(d): The zonal distributions of the overlap parameter for different multilayered cloud types and the cumulative overlap parameter of all multilayered cloud types (gray line).

1148
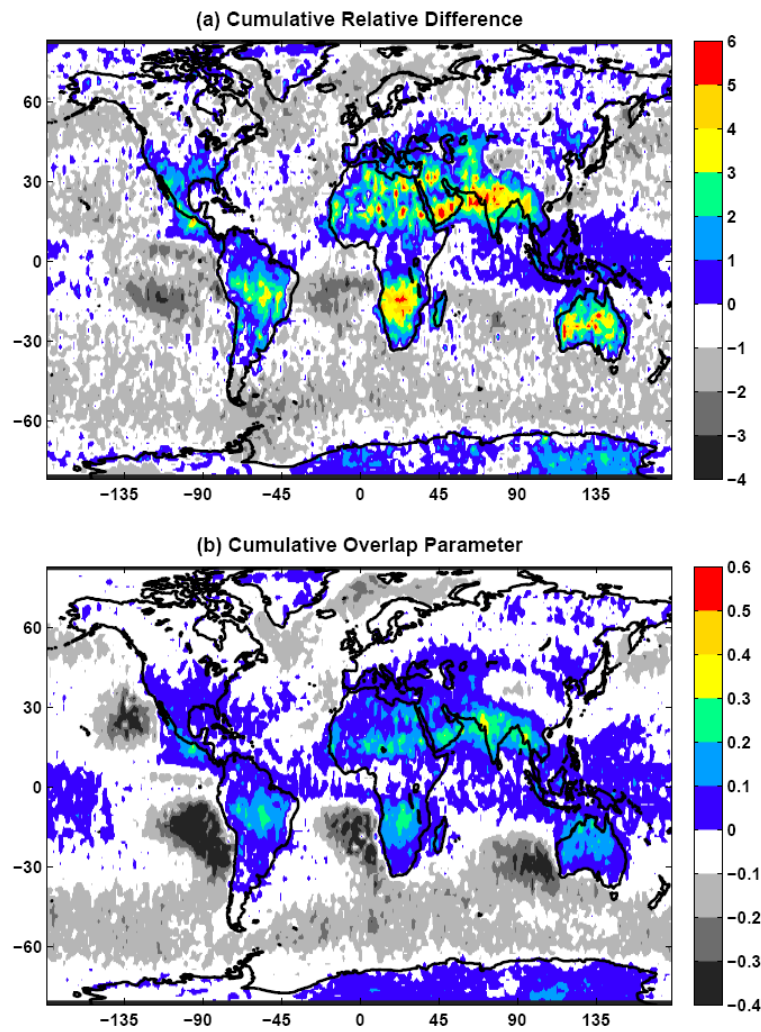
1149

1150

1151

1152

1153

1154

1155

1156

1157

1158

1159

1160

1161

1162

(a) Cumulative Relative Difference

(b) Cumulative Overlap Parameter

1163

Figure 9. The global distributions of (a) the cumulative relative difference and (b) the

cumulative overlap parameter of all multilayered cloud types.